DOI:10.14753/SE.2025.3183

SEMMELWEIS EGYETEM

DOKTORI ISKOLA

Ph.D. értekezések

3183.

SURGUTA SÁRA ESZTER

Molekuláris és experimentális onkológia

című program

Programvezető: Dr. Bödör Csaba, egyetemi tanár

Témavezető: Dr. Tóvári József, biológus, osztályvezető

DOI:10.14753/SE.2025.3183

INVESTIGATING TUMOR CELL MOTILITY UNDER HYPOXIA AND THERAPEUTIC RESISTANCE IN CANCER MODELS

PhD thesis

Sára Eszter Surguta

Pathology and Oncology Division

Semmelweis University

Supervisor: József Tóvári, D.Sc

Official reviewers: Marcell Attila Szász, MD, Ph.D
Margit Balázs, MD, D.Sc

Head of the Complex Examination Committee:

Prof. Janina Kulka, MD, D.Sc

Members of the Complex Examination Committee:

Henrietta Butz, MD, Ph.D

Katalin Erdélyi, Ph.D

Budapest
2025

DOI:10.14753/SE.2025.3183

Table of Contents

DOI:10.14753/SE.2025.3183

DOI:10.14753/SE.2025.3183

List of Abbreviations

ALK	Anaplastic lymphoma kinase
BRAFi	BRAF inhibitor
BSA	Bovine serum albumin
DMEM	Dulbecco's Modified Eagle Medium
ECM	Extracellular matrix
EDTA	Ethylenediaminetetraacetic acid
EGFR	Epidermal growth factor receptor
EMT	Epithelial-mesenchymal transition
FAK	Focal Adhesion Kinase
p-FAK	Phosphorylated Focal Adhesion Kinase
FBS	Fetal Bovine Serum
HIF	Hypoxia-inducible factor
HRE	Hypoxia-response element
IFI27	Interferon alpha inducible protein 27
IL-2	Interleukin-2
LUAD	Lung adenocarcinoma
PARP	Poly (ADP-ribose) polymerase
PBS	Phosphate-buffered saline
PD-L1	Programmed Death-Ligand 1
PDTX	Patient-derived tumor xenograft
qPCR	Quantitative Real-Time Polymerase Chain Reaction
PHDs	Prolyl Hydroxylases Domain
SCLC	Small cell lung cancer
SDS	Sodium Dodecyl Sulfate
SRB	Cytotoxic Sulforhodamine-B
MAPK	Mitogen-activated protein kinase
MEK	Mitogen-activated protein kinase kinase
MEKi	MEK inhibitor

DOI:10.14753/SE.2025.3183

NF-κB	Nuclear factor k-light-chain-enhancer of activated B cells
NOD-SCID	NOD.CB17-Prkdcscid/NCrCrl
NSCLC	Non-small cell lung cancer
NSG	NOD.Cg-Prkdcscid Il2rgtm1Wjl/SzJ
NTRK	Neurotrophic Tyrosine Receptor Kinase
TGF-β	Transforming Growth Factor beta
TME	Tumor Microenvironment
VHL	Von Hippel-Lindau

DOI:10.14753/SE.2025.3183

1. Introduction

1.1 Incidence and mortality of lung and melanoma cancer patients

Cancer is one of the leading causes of death worldwide, accounting for 9.7 million estimated deaths in 2022. Among malignant diseases in 2022, lung cancer was most frequently diagnosed, responsible for almost 2.5 million estimated new cases globally (1). Furthermore, despite the advances in lung cancer therapies, the 5-year survival rate remains low at 5-15% (2). Poor prognosis is largely due to the lack of obvious symptoms in the early stage and consequent late diagnosis of the advanced, metastatic disease (3).

Malignant melanoma of the skin, while less common, is notably aggressive and has seen rising incidence rates in recent years with 331,647 estimated new cases in 2022 (1). In Hungary, according to the Hungarian National Cancer Registry data, ~10,000 new lung cancer cases (C33-C34) and ~2500-2700 new melanoma cases (C43) were registered in 2020 (4-6).

1.2 Outlines of treatment options

Traditional classifications of lung cancer categorize the disease into two main types: small cell lung cancer (SCLC) and non-small cell lung cancer (NSCLC). Within the NSCLC, three main subtypes are recognized: large cell carcinoma, squamous cell carcinoma, and adenocarcinoma, with adenocarcinoma being the most prevalent subtype. The standard treatment for lung adenocarcinoma patients with stage IB-IIIA involves surgery followed by adjuvant chemotherapy. For patients with stage IV lung adenocarcinoma (LUAD), the treatment approach for immune checkpoint inhibitor therapy is based on PD-L1 expression levels (7). If PD-L1 expression is below 50%, a combination of chemotherapy and pembrolizumab is recommended, conversely, if PD-L1 expression is 50% or higher, pembrolizumab monotherapy may be utilized. Additionally, for tumors harboring driver mutations (such as EGFR, ALK, ROS1, RET, BRAF, NTRK gene fusions, or MET exon 14 skipping), cisplatin-based chemotherapy may be combined with bevacizumab and an oral tyrosine kinase inhibitor or other targeted therapies (8,9).

DOI:10.14753/SE.2025.3183

For advanced, metastatic, unresectable, or recurrent melanoma, surgical excision is often followed by adjuvant chemotherapy. For unresectable malignant melanoma stage III-IV tumors, treatment options include immunotherapy (such as pembrolizumab, nivolumab, ipilimumab, relatlimab, or IL-2), targeted therapy with signal transduction inhibitors (such as the BRAF inhibitors vemurafenib, dabrafenib or encorafenib, MEK inhibitors trametinib, cobimetinib or binimetinib, and the KIT inhibitor imatinib mesylate), as well as traditional chemotherapy agents like dacarbazine, temozolomide, cisplatin, vinblastine, carmustine, tamoxifen, carboplatin and paclitaxel (10,11).

1.3 Challenges in cancer treatment: metastasis and therapy resistance

The most common reason for disease progression and mortality for cancer patients are metastasis formation and resistance against the applied therapy (12). Metastasis is a complex process upon which the malignant cells acquire the capacity to migrate from the primary site, invade surrounding tissues, enter the circulatory system, leave the circulation and form secondary tumors in distant organs (13) **(Figure 1)**. In cancer patients, large numbers of tumor cells enter circulation daily, however, studies in animal models of melanoma indicate that less than 0.1% of these cells successfully metastasize (14). Patients primarily die from metastatic disease, as the presence of a primary tumor alone is rarely enough to cause death.

DOI:10.14753/SE.2025.3183

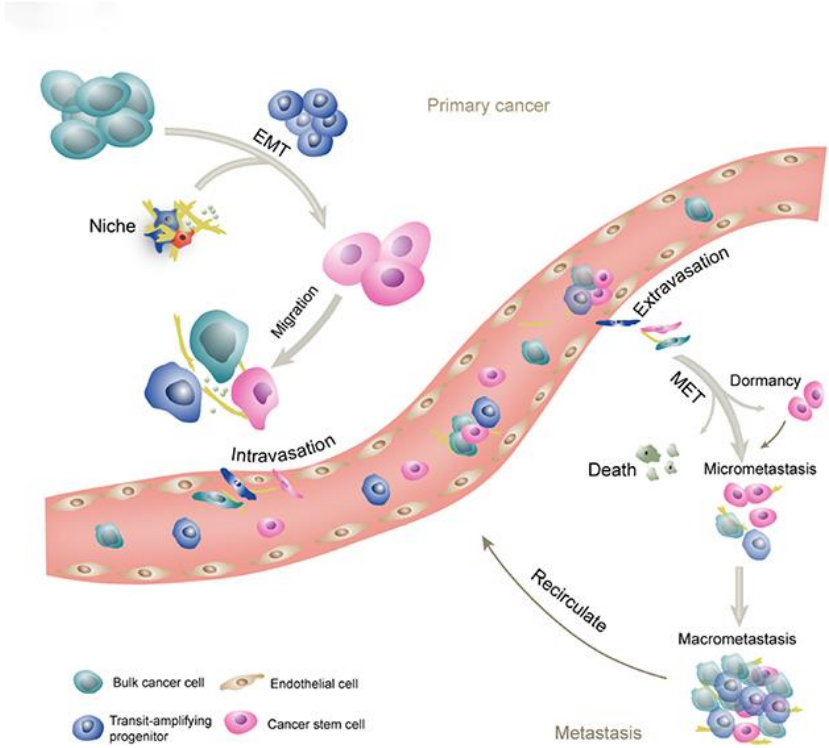

Figure 1. Schematic representation of the metastatic cascade. Figure adapted from He, J. et al. (15).

Drug resistance remains the biggest barrier to achieve cures for patients with cancer. The underlying mechanisms of resistance are as varied as the patients themselves. Each tumor has a unique set of characteristics that drives its progression and can ultimately lead to mortality (16). Therapy resistance can be defined as the ability of cancer cells to withstand the effects of treatment, reduce, or eliminate the treatment's effectiveness resulting in tumor growth or progression. Cancer drug resistance can be divided into two main types: intrinsic and acquired resistance. Intrinsic resistance - often referred to as primary resistance - is characterized by the inherent ability of cancer cells to resist treatment prior to any therapeutic exposure (17,18). Acquired resistance develops when cancer cells gain the ability to resist treatment after initially responding well (19). The mechanisms underlying acquired resistance include the interaction of genetic factors and non-genetic contributors such as genetic diversity, rewiring of compensatory or bypass pathways, and epigenetic modifications. Among the non-genetic contributors to cancer therapeutic resistance, several factors play a significant role, including intratumoral heterogeneity, tumor cell plasticity and the DNA repair mechanisms (20, 21).

DOI:10.14753/SE.2025.3183

1.4 BRAF Inhibitors: Mechanisms and potential approaches to resistance development

The mitogen-activated protein kinase (MAPK) signaling pathway is a key cell signaling pathway involved in the regulation of cell growth, proliferation and survival. In 2002, Davies H. and colleagues made a major breakthrough when they discovered that mutations in the BRAF gene - a key player in the MAPK pathway - are present in many types of cancer (22). Approximately half of melanoma patients have a BRAF mutation (23) that occurs in a single codon, at position 600. This mutation replaces valine with glutamic acid (V600E mutation) (24). This abnormal protein in primary melanomas triggers the activation of the MAPK/ERK pathway, driving the proliferation of cancer cells. The first BRAF inhibitor (BRAFi) vemurafenib was approved in 2011 (25). BRAFi include vemurafenib, dabrafenib and encorafenib, often applied in combination with MEK inhibitors (MEKi) trametinib, cobimetinib, or binimetinib in clinics (26,27). Vemurafenib is effective in BRAF V600E mutant cells by blocking ERK phosphorylation. In contrast, MEKi also block ERK phosphorylation but do so regardless of the cellular genotype (28). The inhibition of BRAF, MEK, or both together in combination has proven highly effective in achieving antitumor effects (29). Unfortunately, cancer cells often develop acquired resistance over time, thwarting all therapeutic efforts (30). To date, the literature on the potential mechanisms of resistance to BRAFi has been overly focused on models based on cell lines. Pathways that may contribute to tumor cell resistance to vemurafenib in melanoma and other kinase-driver tumors include activation of alternative signaling pathways that bypass the MAPK pathway, reactivation of MAPK signaling, or other less well-understood processes (31) **(Figure 2)**.

DOI:10.14753/SE.2025.3183

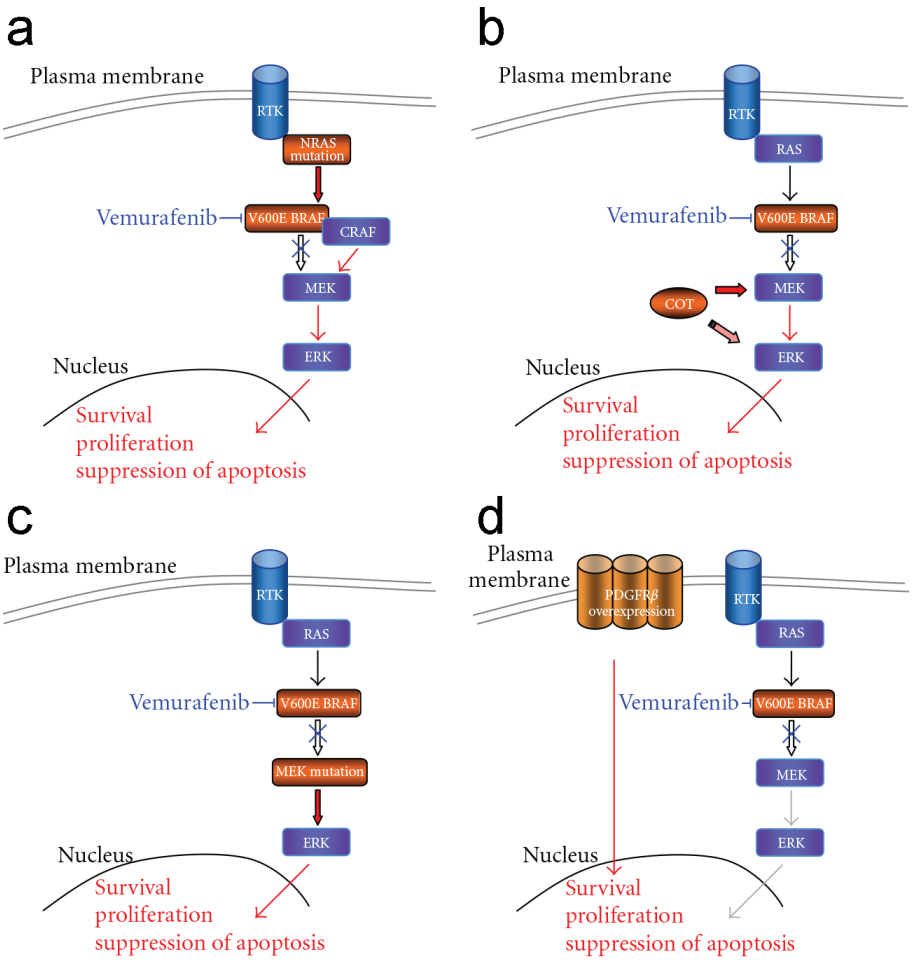

Figure 2. Potential resistance mechanisms against vemurafenib. a) Novel mutations in NRAS lead to BRAF/CRAF heterodimerization, resulting in the reactivation of the MAPK signaling pathway. Enhanced ERK activation without RAF stimulation **b)** by overexpression of COT or **c)** through additional mutations in MEK. **d)** PDGFRβ overexpression can lead to resistance through a mechanism independent of MAPK pathway inhibition. Figure adapted and modified from Ades, F. et al. (32).

These alternative pathways take place in order to restore cell proliferation and avoid apoptotic cell death. However, these models represent isogenic, clone-like cancer cells lacking tumor heterogeneity and the tumor microenvironment. Patient-derived tumor xenograft (PDTX) models have proven to be the most effective preclinical approach to mimic intratumoral cancer heterogeneity, preserve the intrinsic architecture of tumors and study drug response and resistance mechanisms (33). Several studies have explored the utility of PDTX models in tracking acquired resistance to BRAFi. For example, Kemper and colleagues conducted a comprehensive analysis of clinical samples from 89 patients, obtaining surgical samples from both treatment-naive and treatment-

resistant tumors. They successfully established and evaluated PDTX tumors, discovering that duplication of the BRAF V600E kinase domain can lead to resistance. Notably, this resistance was reversible through treatment with a pan-RAF dimerization inhibitor in mouse models (34).

1.5 Tumor hypoxia

Over the past two decades, it has become evident that the tumor microenvironment (TME) plays an equally critical role in modulating tumor aggressiveness, motility, metastasis and the development of resistance to therapies (35), alongside the genetic aberrations that were initially thought to be the primary drivers of tumor initiation and progression (36). Among the tumor microenvironmental factors, it is important to highlight hypoxia, as it has been suggested to play a crucial role in tumor progression and metastasis formation (37). Therefore, investigation the molecular mechanisms behind the development of lung cancer under hypoxia is crucial to establish more rational therapeutic approaches for the treatment of LUAD patients. Hypoxia, or oxygen deprivation, is a common phenomenon in the majority of malignant solid tumors, influenced by various factors such as tumor size, stage, heterogeneity, and the initial oxygenation of the tissue (38,39). For instance, the median oxygen level in healthy lung tissue is approximately 5.6% O_2, whereas hypoxic tumor tissue in lung cancer patients typically exhibits oxygen levels between 1.9% and 2.2% O_2 (40).

Tumor hypoxia can be classified into three types based on duration: acute, chronic, and intermittent hypoxia. Acute hypoxia refers to short-term exposure (less than 24 hours) to environments with 1% O_2 or less (41), while chronic hypoxia is characterized by prolonged exposure (more than 24 hours) to low oxygen levels. Both acute and chronic hypoxia can occur intermittently, displaying cycles of reoxygenation and hypoxic conditions (42). The molecular response to hypoxia is primarily mediated by a family of transcriptional regulators known as hypoxia-inducible factors (HIFs), which have been recognized for over three decades (43). Under hypoxic conditions, hypoxia-inducible factor 1-alpha (HIF-1α) forms a heterodimeric transcription factor with HIF-1β subunit and translocates to the nucleus (44) **(Figure 3).** All three members of the HIF family - HIF-1, HIF-2, and HIF-3 - (45) can bind to hypoxia-response elements (HREs), activating

transcriptional responses in a cell type-specific manner that regulate hypoxia signaling and help maintain cellular oxygen homeostasis (46,47). Under normoxic conditions the proline residues of the HIF-1α subunit are hydroxylated by the prolyl hydroxylase domains (PHDs), which promotes the binding of the von Hippel-Lindau protein (VHL) leading to its proteasomal degradation (48) **(Figure 3)**.

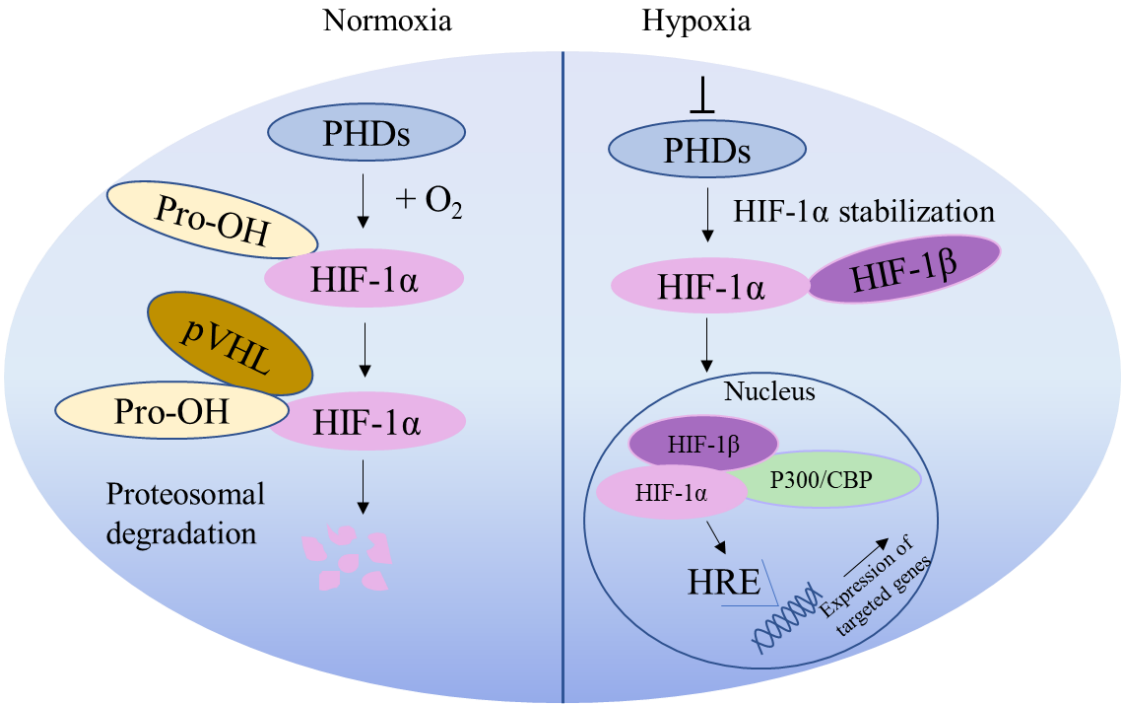

Figure 3. Representative image of the role of HIF-1α under normoxic and hypoxic conditions. Under normoxia, HIF-1α undergoes ubiquitination and proteasomal degradation, while in hypoxic conditions, it binds to HIF-1β, translocates to the nucleus, binds to the HRE region of DNA, and regulates the transcription of hundreds of genes. Figure was prepared by the author.

Various methods are available for stabilizing the HIF protein, facilitating both *in vitro* and *in vivo* research. For example, $CoCl_2$ is a typical hypoxia-mimicking agent, used in numerous studies (49). The mechanism of the $CoCl_2$ is characterized by inhibiting the interaction between HIF1α and the VHL protein, thereby preventing the degradation of HIF1α. The cellular response to hypoxia is not only dependent on HIFs, various other transcription factors, notably the Nuclear Factor-κB (NF-κB) family, also play significant roles. NF-κB activation in cancer cells exposed to hypoxic conditions typically leads to decreased apoptosis and enhanced angiogenesis. However, the precise mechanism leading to NF-κB activation in hypoxia is still under investigation (50,51).

1.6 Epithelial-mesenchymal transition (EMT)

One major metastasis-promoting cellular process that hypoxia can modulate is the epithelial-mesenchymal transition (EMT). The EMT is driven by transcription factors including Twist, Snail, Slug, and Zeb1. These factors mediate EMT through activation of key signaling pathways, with the transforming growth factor-beta (TGF-β), Wnt, and Notch pathways (52). In general, during EMT, cells lose the expression of certain epithelial markers such as E-cadherin, while increasing the expression of mesenchymal markers like N-cadherin or vimentin (53,54). Cells that undergo EMT gain mesenchymal-like behavior, facilitating their migration away from the primary tumor site through various migration strategies (55), including multicellular, collective, and single-cell mesenchymal migration (56).

1.7 Tumor cell migration and invasion

Several factors within the tumor microenvironment play a crucial role in regulating cancer cell migration and invasion. Key contributors include hypoxia, the presence of chemoattractants, extracellular matrix (ECM) stiffness, and nutrient deprivation; all of which create conditions that drive cancer cells to adapt and invade surrounding tissues (57).

Tumor cells exhibit diverse migration patterns when infiltrating surrounding tissues, primarily categorized as individual cell migration and collective migration. Individual cell migration (mesenchymal, amoeboid, chain) involves tumor cells disseminating as single entities, commonly seen in hematological malignancies like leukemias and lymphomas, as well as some solid tumors such as sarcomas. In contrast, collective migration occurs when tumor cells move together, a mechanism frequently observed in epithelial tumors, often facilitated by complete or partial EMT and influenced by the ECM. Many tumors display both migration types simultaneously, reflecting cellular heterogeneity, less differentiated tumor cells are more prone to individual migration, while more differentiated cells typically move collectively (55,56).

Numerous studies aimed to investigate the effects of hypoxia on cell motility *in vitro*; however, these findings are often conflicting and utilized varying experimental

DOI:10.14753/SE.2025.3183

setups (58). Thus, further studies are urgently needed for better understanding of this crucial process in tumor progression.

DOI:10.14753/SE.2025.3183

2. Objectives

In this study, we aimed to investigate the followings:

1) The effects of reduced oxygen level (hypoxia) or hypoxia mimicking ($CoCl_2$ treatment) on the expression of hypoxia-related proteins and genes in lung adenocarcinoma.
2) The impact of hypoxia and $CoCl_2$ exposure on the single-cell and collective migration ability of LUAD cells.
3) Identifying resistance-associated changes using RNA sequencing in *in vivo* PDTX model of vemurafenib-resistant malignant melanoma.
4) Validating the identified expression differences at RNA and protein level.

DOI:10.14753/SE.2025.3183

3. Methods

3.1 Cell culture

Human lung adenocarcinoma cell lines PF901, PF139, H838 and H1975 were cultured in DMEM (Dulbecco's Modified Eagle Medium; Lonza, Basel, Switzerland); containing 4500 mg/dm^3 glucose, pyruvate and L-glutamine) supplemented with 10% FBS (Fetal Bovine Serum; EuroClone, Pero, MI, Italy), 1% penicillin/streptomycin solution (Lonza) and incubated at 37°C in a humidified 5% CO_2 atmosphere. Cells were cultured in 1% O_2, 5% CO_2 and 94% N_2 for hypoxia measurements to mimic the hypoxic environment. H838 cells were purchased from Horizon Discovery Ltd (Waterbeach, UK) while H1975 cells derived from ATCC (Manassas, Virginia, USA). PF139 and PF901 cells were established from malignant pleural effusion samples in cooperation with the West German Biobank Essen as described earlier (59,60). The patients provided written informed consent, and the experiments were approved by the Ethics Committee of the University Hospital Essen (#18-8208-BO). All experiments were performed in accordance with relevant guidelines and regulations.

3.2 Videomicroscopy

Videomicroscopy was performed with 4x10^2 cells/well seeding concentration in 24-well cell culture plates (Greiner AG, Kremsmünster, Austria). The day after the cells were plated, the medium was replaced with fresh medium (complemented with 10% FBS and 1% p/s) with or without 200 µM $CoCl_2$ (Sigma-Aldrich St. Louis, Missouri, USA). Preliminary experiments by our group had shown that no cytotoxicity occurred at this concentration (58). Two independent wells were monitored for each experiment for normoxia and 200 µM $CoCl_2$ treatment, while four independent wells were monitored for hypoxia. One field of view per well was imaged every 10 min during the 48 hours treatment period using a zenCellowl incubator microscope (innoME, Espelkamp, Germany).

For cell migration, videos were analyzed using CellTracker_v1_1_1 Standalone Version free software (61). Migratory activity of cells was measured using the semi-automatic tracking function of the software (Vignetting correction settings: Bicubic

interpolation; Block size=100; Maximum allowed displacement=20; Semi-automatic tracking settings: Template matching; Maximum allowed displacement=20; Cell diameter=50). The resulting trajectories were checked and corrected if necessary using the manual function of the software. Following this step, data generated by the software were exported to an excel spreadsheet for further analysis. Results from three independent experiments were used for the calculations. Data were divided into 12-hour intervals (1-72, 73-144, 145-216, 217-288 frames) and were further analyzed using the free software Chemotaxis and Migration Tool (Ibidi, Gräfelfing, Germany). Briefly, distance from origin and total length data were obtained from trajectories of the cells that remained in the field of view through the given time interval. The results were plotted and statistically evaluated using GraphPad Prism 5 software (La Jolla, San Diego, CA, USA).

3.3 Cytotoxic Sulforhodamine-B (SRB) assay

In brief, the cells were seeded in a 96-well plate at a concentration of 1×10^2 or $1x20^3$ cells/well in 200 µL fresh completed DMEM (Lonza) (medium supplemented with 10% FBS (EuroClone), 1% penicillin/streptomycin solution (Lonza)) and left to attach to the plates for 24 hours. Then, cells were incubated at 37°C in a humidified 5% CO_2 atmosphere or for hypoxic conditions, cells were incubated in 1% O_2, 5% CO_2 and 94% N_2 for 48 hours. After that, the cells were washed and fixed with 100 µL cold 10% trichloroacetic acid for 1h at 4ºC. The wells were then washed 2 times with distilled water and stained for 15 min at room temperature with 70 µL 0.4% SRB dissolved in 1% acetic acid. Then, cells were washed with 1% acetic acid 3 times. The plates were air-dried and the dye was solubilized with 200 µl/well of 10 mM tris base (pH 10.5) for 10 min. The optical density (O.D.) of each well was measured spectrophotometrically at 570 nm with BioTek 800 microplate reader (Agilent, Santa Clara, CA) with automatic shaking for 30 seconds before reading. The mean background absorbance was subtracted automatically and mean values for each condition were calculated. Three independent biological replicates were performed.

3.4 Scratch assay

Scratch assays were prepared using the MuviCyte™ live-cell Imaging System (PerkinElmer, Waltham, MA, USA) supplied with a MuviCyte™ scratcher (PerkinElmer)

to perform standardized scratches on 96 well plates following the manufacturer's instructions. Briefly, cells were seeded at $4x10^4$ cells/well density and left for overnight to attach. The next day, scratches were made using the MuviCyte™ scratcher device and wells were washed with DPBS to remove debris. DPBS was replaced with fresh DMEM completed with 10% FBS and 1% p/s. Wound closure was monitored in four parallel wells for each cell line for 72-hour period. Pictures were taken from each well in every 6 hours. Analysis of wound closure were performed using a modified script from Suarez-Arnedo, A. and colleges (62) for ImageJ Fiji software. The script automatically measures the area of the scratch for different time points. Data were normalized and expressed as the percentage of the starting scratch area. For each experiment, data from the four independent wells for each cell line were averaged and used as a single replicate, graphed in GraphPad Prism 5 software. Three independent biological replicates were performed. $T_{1/2}$ wound closure data was calculated with GraphPad Prism 5 software using nonlinear regression (log inhibitor vs normalized response, variable slope).

3.5 Western blot

The effects of $CoCl_2$ treatment or hypoxia on protein expression and activation were investigated by immunoblot analysis. Cells were plated on 6-well plates (Greiner AG) at $2x10^5$ cell/well density and were exposed to normoxia, normoxia + 200 µM $CoCl_2$ treatment or hypoxia for 48 hours. At the end of the treatment period, cells were washed with DPBS and were fixed with 6% trichloroacetic acid for 1 hour at 4°C. Cells were then mechanically scraped and centrifuged at 6000 RCF for 15 minutes. The precipitated protein was dissolved in a modified Läemmli-type buffer containing 0.02% bromophenol blue, 10% glycerol, 2% SDS, 100 mM dithiothreitol (DTT), 5 mM EDTA, 125 mg/ml urea, 90 mM Tris-HCl, pH 7.9. A Qubit fluorometer (Invitrogen™ Waltham, Massachusetts, USA) was used to determine protein concentration. Following this step, equal amounts of protein (20 µg/lane) from each sample were loaded to a 10% polyacrylamide gel and blotted onto PVDF membranes after electrophoretic separation using 10% precast polyacrilamide gels and Turbo-Blot system (BIO-RAD). Hypoxic response was evaluated by assessing changes in the protein level of HIF-1α (1:1000) (D5F3M, Cell Signaling Technology Danvers, MA, US), PARP (1:1000) (9542, Cell Signaling Technology), p-Histone H3 (1:1000) (9701S, Cell Signaling Technology), p-

FAK (1:1000) (3283 Cell Signaling Technology), β-tubulin (1:1000) (2128T, Cell Signaling Technology), FAK (1:1000) (3285T, Cell Signaling Technology), p38 (1:1000) (8690S, Cell Signaling Technology), p-p38 (1:1000) (4511, Cell Signaling Technology). Primary antibodies were used to detect changes in apoptosis and cell proliferation, respectively. All antibodies were dissolved in 5% BSA (bovine serum albumin) or nonfat dry milk in 1x TTBS (Tris-buffered saline supplemented with 1% Tween80) buffer according to the manufacturer's instructions. Membranes were blocked at room temperature (RT) for one hour in 5% milk dissolved in 1x TTBS and incubated overnight at 4°C with primary antibodies. HRP-conjugated rabbit secondary antibody (1:10000, 1 hour, RT) and Pierce ECL Western Blotting Substrate (Thermo Fisher Scientific, Waltham, MA, USA) were used for signal development. Ponceau total protein staining was used for normalization. Quantitation was performed using ImageLab (Bio-Rad Hercules, CA, USA) software. All four cell lines were analyzed in 3 biological replicates.

Protein expressions in PDTX samples were carried out from flash-frozen tissue samples. We used frozen grinding (sterile manual grinder, frozen with continuous addition of liquid nitrogen, pulverizing the sample), and the resulting tissue-powder was immediately put to ice with 200 µl of Mg^{2+} lysis buffer containing aprotinin, leupeptin and phosphatase inhibitor PMSF. Gel electrophoresis and western blotting were performed according to the manufacturer’s protocol in 1mm 10% SDS polyacrylamide gels, and Turbo-Blot semi-dry blotting system (Bio-Rad). Membranes were blocked for 1 hour with 5% nonfat dry milk dissolved in TBS tween, then incubated in the primary antibodies overnight (4°C). After washing and secondary labeling (1 hour, RT), HRP signals were visualized with WesternBright ECL system (Advansta, San Jose, CA, USA) and documented with iBright 750 documentation system (Thermo Fisher, Waltham, MA, USA). Antibodies used: AKT: #4691 (1:1000); p-AKT: #13038 (1:1000); mTOR: #2983 (1:1000); p-mTOR: #5536 (1:1000); p44/42 (ERK1/2): #4695 (1:1000); p-p44/42 (p-ERK1/2) #4370 (1:2000); PDGFRB: #3169 (1:1000); p-MEK 1/2: #9154 (1:1000); p-c-RAF: 217 #9421 (1:1000); p53: #9282 (1:1000); GAPDH: #2118 (1:1000), all from Cell Signaling Technologies (Danvers, MA, USA), CD27 (ab175403) (1:1000), IFI27 (ab171919) (1 µg/ml), both from Abcam PLC (Cambridge, UK), diluted and applied according to the manufacturer’s instructions. Anti-BRAF V600E mutation-specific antibody (clone VE1) was obtained from Ventana Medical Systems (Oro Valley, AZ,

USA) and diluted in nonfat dry milk – TBS tween solution at a concentration of 1.5ug/ml. Secondary anti-mouse (#7076) (1:1000) or anti-rabbit (#7074) (1:1000) IgG antibodies conjugated with HRP were purchased from Cell Signaling and used according to their manual. Three independent biological replicates were performed.

3.6 Real-time reverse transcription PCR

Samples were isolated in TRIzol reagent (Ambion, Life Technologies, Carlsbad, CA, USA) and the Direct-zol™ RNA MiniPrep (Zymo Research) kit was used to isolate RNA according to the manufacturer's protocol. The concentration and purity of the RNA were determined using spectrophotometry at 260/280 and 260/230 nm (NanoDrop One, ThermoFisher Scientific, Madison, WI, USA). The RNA was then reverse transcribed in an Eppendorf 5331 Mastercycler Gradient thermocycler (Eppendorf, Enfield, CT, USA), using a Reverse Transcription System (Promega Corporation, Madison, WI, USA) according to the manufacturer's instructions. The resulting cDNA samples were stored at -80°C until further use. Quantitative real-time PCR reactions were performed using SsoAdvanced Universal SYBR Green Supermix (Bio-Rad, Hercules, CA, USA) in a CFX96™ Real-Time PCR System according to the manufacturer's instructions. For real-time quantitative PCR (qPCR), the used primer sequences are summarized in **Table 1**.

Table 1. Oligonucleotide primers used in the study.

Gene	Forward primer	Reverse primer
vimentin	AGTCCACTGAGTACCGGAGAC	CATTTCACGCATCTGGCGTTC
E-cadherin	ATTTTTCCCTCGACACCCGAT	TCCCAGGCGTAGACCAAGA
N-cadherin	AGCCAACCTTAACTGAGGAGT	GGCAAGTTGATTGGAGGGATG
RPLP0	AGCCCAGAACACTGGTCTC	ACTCAGGATTTCAATGGTG
IFI27	TGCTCTCACCTCATCAGCAGT	CACAACTCCTCCAATCACAACT
CD27	TCAGCAACTGGGCACAGAAA	GGATCACACTGAGCAGCCTT
RPLP0	AGCCCAGAACACTGGTCTC	ACTCAGGATTTCAATGGTGCC

The mRNA expression was analyzed by relative quantification, threshold cycle (C_t) values and $2^{-\Delta\Delta Ct}$ method. Data derived from three independent experiments.

3.7 Immunofluorescent analysis

For immunofluorescent analysis, cells were seeded on glass immunohistological slides in 10% FBS + DMEM droplets. The next day, scratches were made and then cells were cultured for 48 hours in normoxic or hypoxic conditions, then were fixed for 20 minutes in 4% formaldehyde. After fixation, cells were repeatedly washed with PBS, then permeabilized with 0.01% TritonX100 for 5 minutes. Following additional washing steps after permeabilization, cells were incubated with vimentin primary antibody Clone V9 (Agilent, USA) (1:200) for an hour at RT according to the manufacturer's instructions, then were washed in PBS and probed for half an hour with anti-Mouse IgG (H+L) Secondary Antibody, Alexa Fluor™ 488 (10µg/ml) (A-11029, Thermo Fisher Scientific, USA). Nuclei was stained with DAPI, and slides was covered with ProLong Gold antifade reagent (P36930, Thermo Fisher Scientific), then were visualized using an Eclipse E600 (Nikon Optoteam, Vienna, Austria) fluorescent microscope with a CCD camera.

Pictures of cells were analyzed in ImageJ Fiji open-source software. Briefly, a top-hat filter was applied (50 px radius), then the resulting pictures were converted to binary mask. “Median” command of binary transformations was applied (3 px radius), then particles (binary representatives of vimentin expression of each cells) were analyzed (Particle size: 100-4000 pxs). Results were manually revised and segmented, if necessary, based on the original fluorescent images. Area and circularity data were collected from three independent experiments and were graphed with GraphPad Prism 5 software.

3.8 PDTX Animal Model of Vemurafenib Treatment

KINETO Lab Ltd. has license for animal housing (PEI/001/1715/2015) and PDTX sample collection, handling, model generation and use (PE/EA/401-7/2020, IV/10147-1/2020/EKU). The provided PDTX samples were transferred to the experimental animal house of the National Institute of Oncology on dry ice. There, the permissions for animal housing (PEI/001/1738-3/2015) and tumor xenograft experiment with anticancer agents (PE/EA/1461-7/2020) were covering all activities during the study. All ethical permissions were given by the Scientific and Research Ethics Committee, a national board in Hungary. In model generation, the fresh surgical samples were implanted into three 8-week-old NOD.Cg-Prkdcscid Il2rgtm1Wjl/SzJ (NSG) mice

(The Jackson Laboratory, Bar Harbor, ME, USA). Under anesthesia, approximately 5-10 mm^3 tumor tissue pieces were implanted subcutaneously under the right dorsal skin, and wounds were closed with Novosyn 4/0 surgical suture (B.Braun, Melsungen, Germany). Tumor growth was followed, and grown tumors were removed and cut into 5-10 mm^3 pieces. At the animal house of the National Institute of Oncology, serial transplanting was carried out using 8- to 12-week-old NOD.CB17-Prkdcscid/NCrCrl (NOD-SCID) mice, obtained from the animal house of the National Institute of Oncology. When tumor sizes reached approximately 100 mm^3, *per os* treatment was carried out with 100 mg/kg vemurafenib five times a week. Vemurafenib by the commercial name Zelboraf (Roche, Basel, Switzerland) pills were pulverized with a grinder and dissolved in sterile water to reach the concentration of 10mg/ml. The solution was stored at 4°C for not more than a week, and vortexed before every use. When either the tumor sizes reached 1500-2000 mm^3 or the animals reached the age of about 6 months (treated groups), the tumors were removed, and spread as follows: from one tumor, half of the tissue was serially transplanted into new young animals, the rest of the tumors were snap-frozen within 10 minutes to ensure RNA and protein integrity and kept at -80°C until further use.

3.9 Data processing and statistical analysis

Statistical analyses were performed by Graphpad Prism 5 software. Briefly, single-cell motility data were analyzed for normal distribution using the Shapiro-Wilk test. As the number of data points was too small for Shapiro-Wilk test in case of proliferation data, we employed the Kolmogorov-Smirnov test to examine the normal distribution for this dataset. Datasets with normal distribution were analyzed by ANOVA followed by Tukey's Multiple Comparison test, otherwise Kruskal-Wallis test was applied followed by Dunn's Multiple Comparison test. Data from scratch assays were analyzed using non-linear regression and compared with the sum-of-squares F test comparing Hillslope and $logIC_{50}$ data. RNA and protein expression data were analyzed using the unpaired t-test with Welch correction. Tumor growth data was documented and graphed using Microsoft Excel. The relative expression levels in qPCR were evaluated by the CFX Maestro software package (Bio-235 Rad), while graphs and Student's t-tests were applied in Microsoft Excel.

DOI:10.14753/SE.2025.3183

4. Results

4.1 *In vitro* modeling of the migration ability and changes in EMT markers of LUAD cell lines under hypoxic conditions

4.1.1 The effect of hypoxia and $CoCl_2$ on hypoxia-related protein expression

A panel of lung adenocarcinoma cell lines was selected, each harboring major mutation commonly found in LUAD tumors. Specifically, this panel includes cell lines with mutations in the oncoproteins EGFR (H1975), KRAS (PF139), and BRAF (PF901). Additionally, one cell line (H838) was also included that does not possess any known driver mutations.

First, we performed immunoblot analysis to follow changes in HIF-1α, NF-κB, and phosphorylated NF-κB levels as a primary regulator for cellular adaptation to hypoxia. Also, we aimed to determine whether apoptosis occurs by assessing the presence of cleaved PARP in *in vitro* cultured LUAD cells exposed to $CoCl_2$ treatment or hypoxic conditions (1% O_2 level) **(Figure 5)**. As a key signaling hub activated by hypoxia, HIF-1α was found to be upregulated across all cell lines when subjected to either hypoxia or $CoCl_2$ (hypoxia-mimicking) treatment. $CoCl_2$ acts as a hypoxia-mimetic agent, effectively blocking the physiological degradation of HIF-1α, which leads to its stabilization and accumulation within the cells. Interestingly, while we observed no significant changes in total NF-κB levels, the levels of its phosphorylated form slightly decreased across all examined cell lines upon hypoxia. Importantly, our analysis revealed that neither treatment condition induced apoptosis in any of the cell lines, as indicated by the absence of detectable cleaved PARP signals **(Figure 5)**.

DOI:10.14753/SE.2025.3183

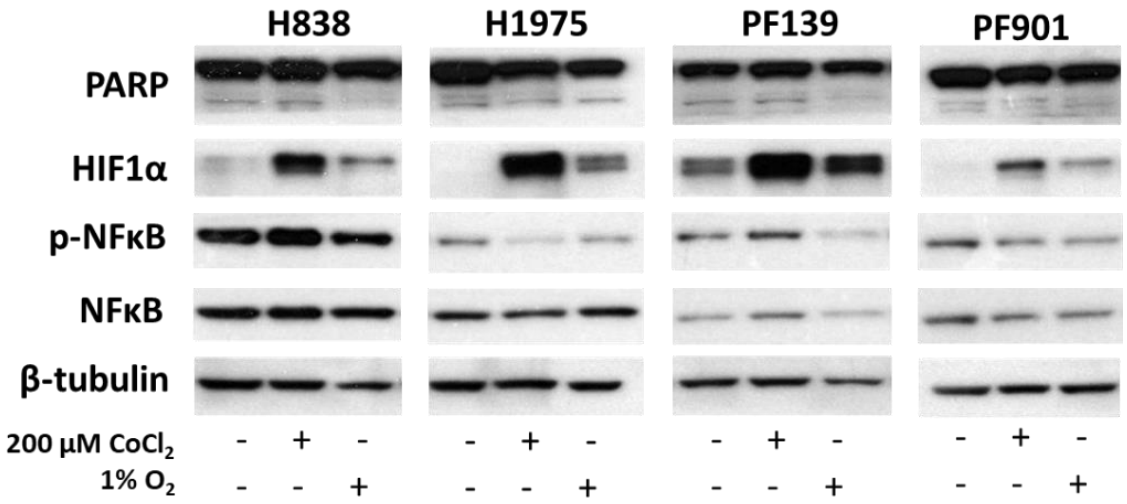

Figure 5. Effect of hypoxia and $CoCl_2$ treatment on HIF-1α, NF-κB, p-NF-κB and apoptosis-related protein expression. Cells were exposed to normoxic (21% O_2 control) or hypoxic (1 % O_2) conditions or 200 µM $CoCl_2$ treatment (21% O_2) for 48 hours. a) Representative Western blot images showing protein level changes upon different conditions. Data derived from three independent experiments. Figure adapted from the author's original publication (63).

4.1.2 The effect of hypoxia on cellular proliferation

After establishing that apoptosis was not induced under hypoxic conditions, our next intriguing question was whether our treatment conditions affect cell proliferation. Therefore, we performed SRB viability assay and immunoblot analysis of the p-Histone H3 proliferation marker protein. Compared to normoxic conditions, under 1% O_2 we did not detect any significant changes regarding the viability of the cells **(Figure 6b)**, however, we observed reduced p-Histone H3 protein expression upon hypoxia **(Fig 6a,c)**.

DOI:10.14753/SE.2025.3183

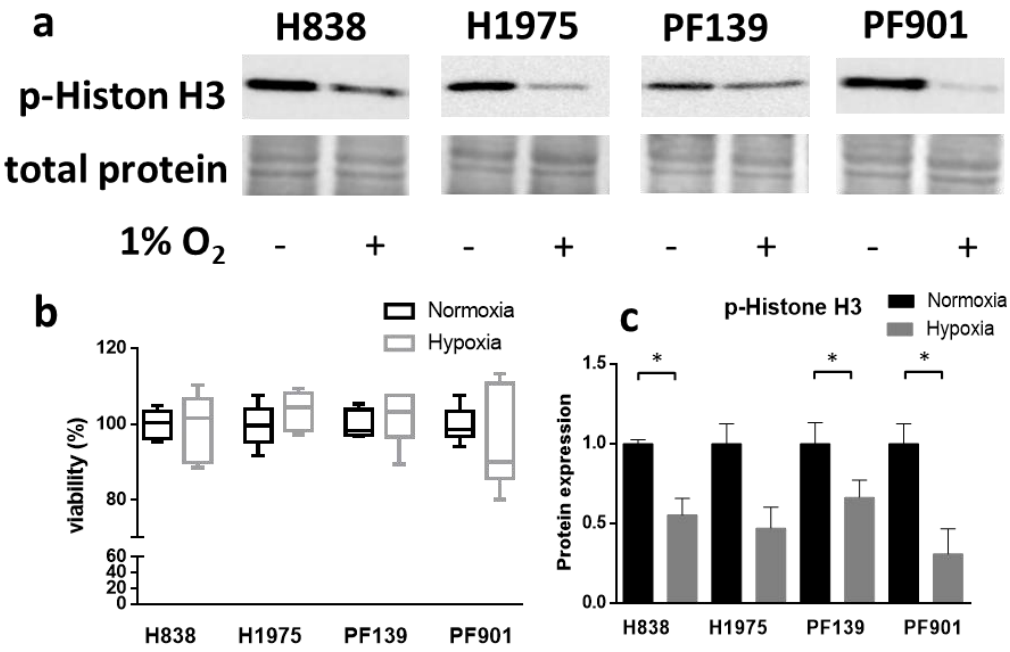

Firgure 6. Changes in cell proliferation and p-Histone H3 protein levels under hypoxic conditions. a) Representative Western blot images demonstrating the alterations in p-Histone H3 protein levels in response to hypoxia. b) Graph show the proliferation data obtained from SRB viability assay c) Graph shows the densitometric evaluation of investigated p-Histone H3 protein, normalized to total protein and expressed relative to control (normoxic sample). Data derived from three independent experiments plotted as mean ± SD. Asterisks show statistically significant differences. Statistical significance was established using unpaired t-test with Welch correction at $p<0.05$. Figure adapted from the author's original publication(63).

4.1.3 The effect of hypoxia on important signaling pathways

Next, we aimed to investigate the potential changes in the activation of key signaling pathways in response to hypoxic conditions. Specifically, we focused on the activation levels of FAK, p38 and SRC. The level of p-SRC decreased in all three cell lines harboring driver mutations, significantly in H1975 and PF901, while no change was observed in the H838 cell line **(Figure 7a,b)**. Although the total P38 level remained unchanged, the phosphorylated form significantly decreased in response to hypoxia across three examined cell lines **(Figure 7b)**. Regarding FAK, there were no changes in either the total or phosphorylated forms across three cell lines. However, in PF139, there

DOI:10.14753/SE.2025.3183

was a slight increase in the total FAK level, accompanied by a visible rise in its phosphorylated form **(Figure 7)**.

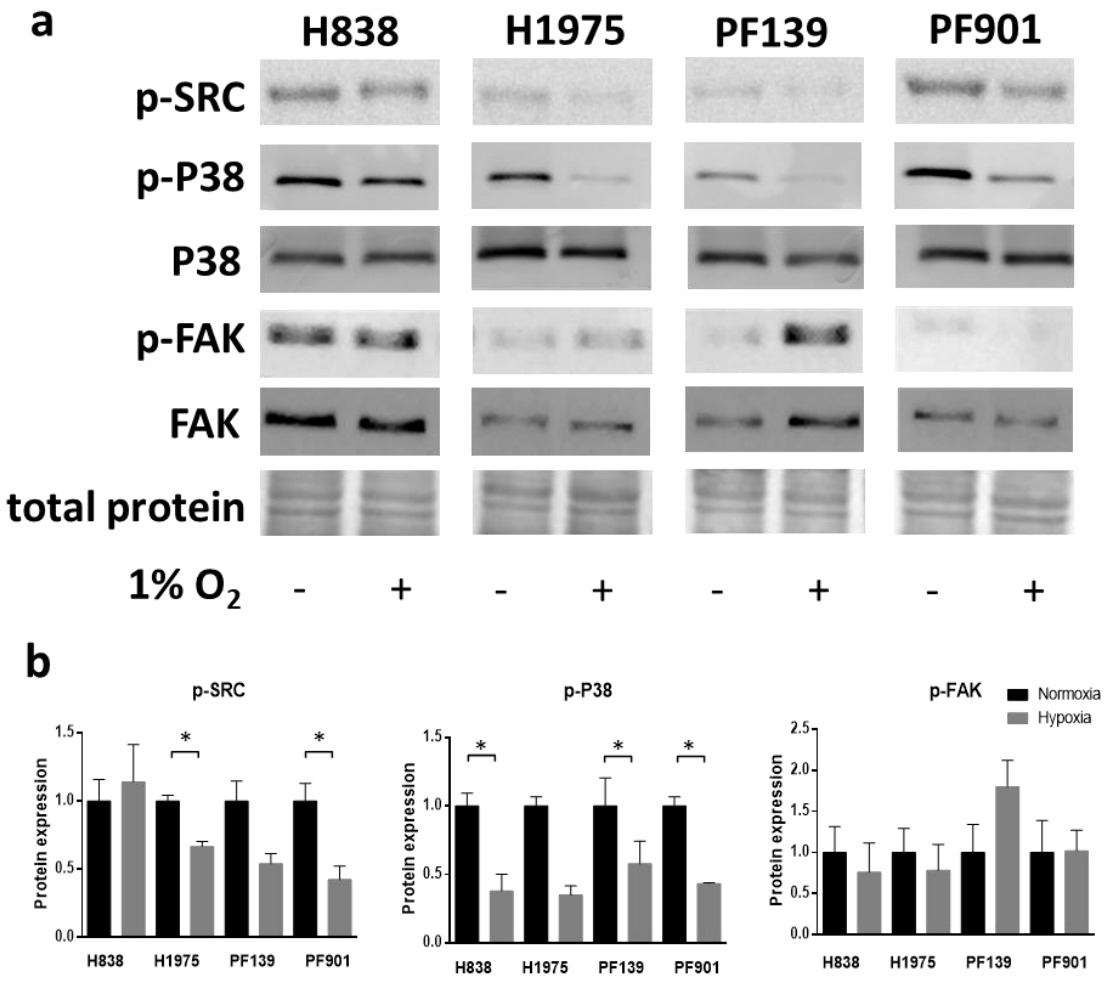

Figure 7. Changes in important signaling pathway protein levels under hypoxic conditions. a) Representative Western blot images showing p-SRC, P38, p-P38, FAK and p-FAK level changes upon hypoxic conditions. b) Graph shows the densitometric evaluation of investigated p-SRC, p-FAK and p-P38 protein, normalized to total protein and expressed relative to control (normoxic sample). Data derived from three independent experiments plotted as mean ± SD. Asterisks show statistically significant differences. Statistical significance was established using unpaired t-test with Welch correction at $p<0.05$. Figure adapted from the author's original publication (63).

DOI:10.14753/SE.2025.3183

4.1.4 Effect of hypoxia on single-cell migration ability

To investigate the impact of hypoxia on the migratory activity of individual tumor cells across the four cell lines, we performed time-lapse videomicroscopy. The tumor cells were allowed to migrate for 48 hours under three different conditions: normoxia (21% O_2), exposure to 200 µM $CoCl_2$ (21% O_2), and hypoxia (1% O_2). Significant differences were observed in the migratory capacities of the four cell lines **(Figure 8)**. Overall, treatment with $CoCl_2$ did not influence cellular motility in any of the cell lines. However, under hypoxic conditions, three out of four cell lines exhibited decreased motility **(Figure 8a)**. Differences in base motility between cell lines, as well as effects of hypoxia were illustrated in a figure displaying the cell trajectories, with trajectories exceeding a specified cut-off value (as shown in each image and adjusted to the speed of the given cell line) highlighted in red **(Figure 8b)**.

DOI:10.14753/SE.2025.3183

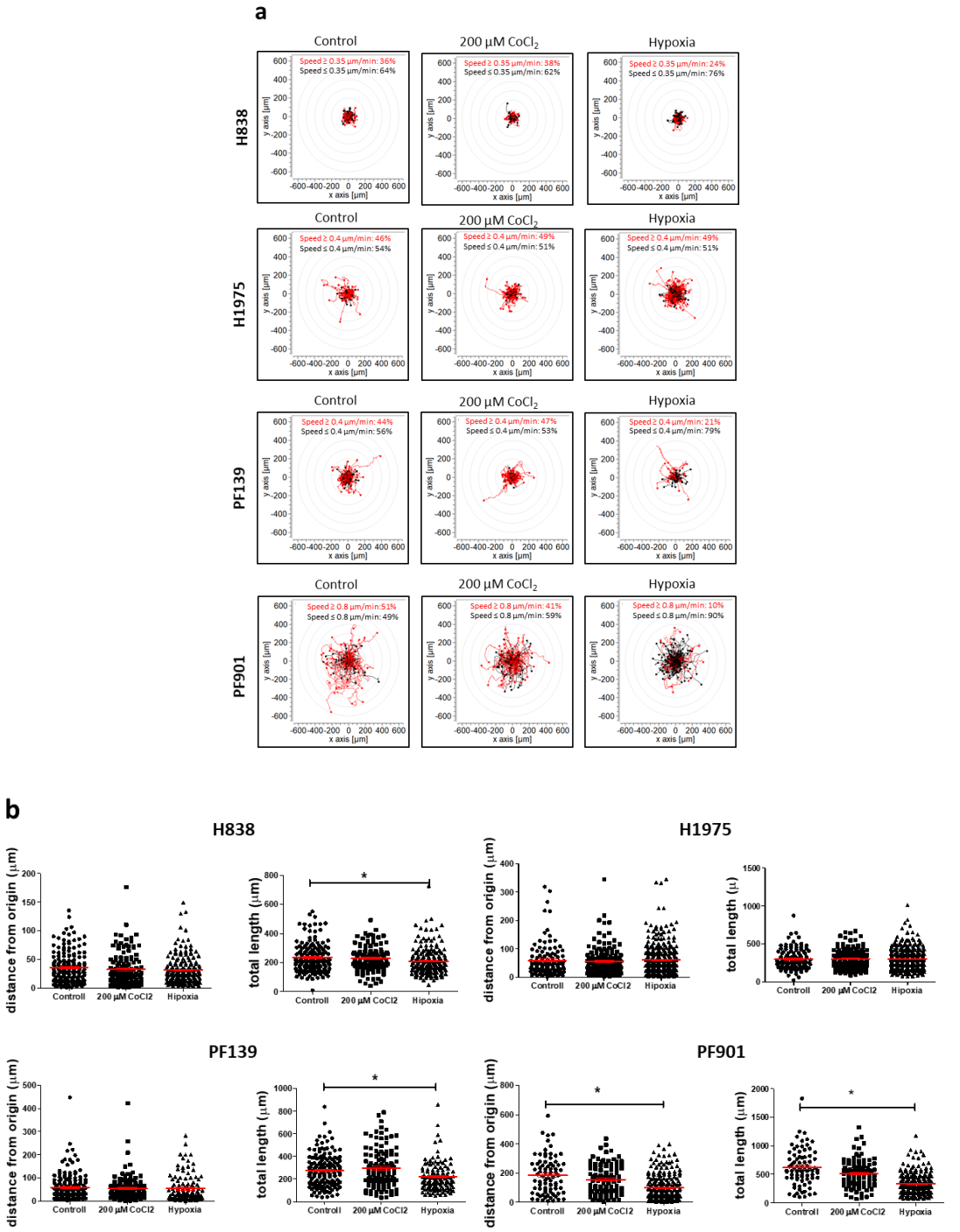

Figure 8. Effects of hypoxia on single-cell motility. a) Motility of individual cells in the last 12-hour frame of the 48-hour-long exposure to normoxia (21% O_2), 200 µM $CoCl_2$, and hypoxia (1% O_2). Only cells that were presented in the video throughout the entire duration were included in the analysis. The distance from the origin and the total length are plotted. b) The images illustrate the trajectories of the corresponding cells shown in panel (a). Note the differences in baseline motility of the distinct cell lines. Asterisks mark statistically significant differences at $p<0.05$. Data is derived from three independent

experiments. Two independent wells were monitored for each experiment for normoxia and 200 µM $CoCl_2$ treatment, while four independent wells were monitored for hypoxia. Kruskal-Wallis test was used followed by Dunn's multiple comparison post-test. Data plotted as mean ± SEM. Figure adapted from the author's original publication (63).

The H838 cell line, which is the least motile among the examined cell lines, exhibited significant differences in its migratory behavior. During the initial 12 hours, its motility increased compared to the control, however, this movement decreased during the subsequent 12-hour period **(Figure 9a)**. The H1975 cell line showed consistent results regardless of the distinct conditions tested, with no changes observed in its motility. **(Figure 9b)**. Hypoxia led to a significant reduction in single-cell migration for both the PF139 and PF901 cell lines throughout the whole time of the experiment **(Figure 9c-d)**.

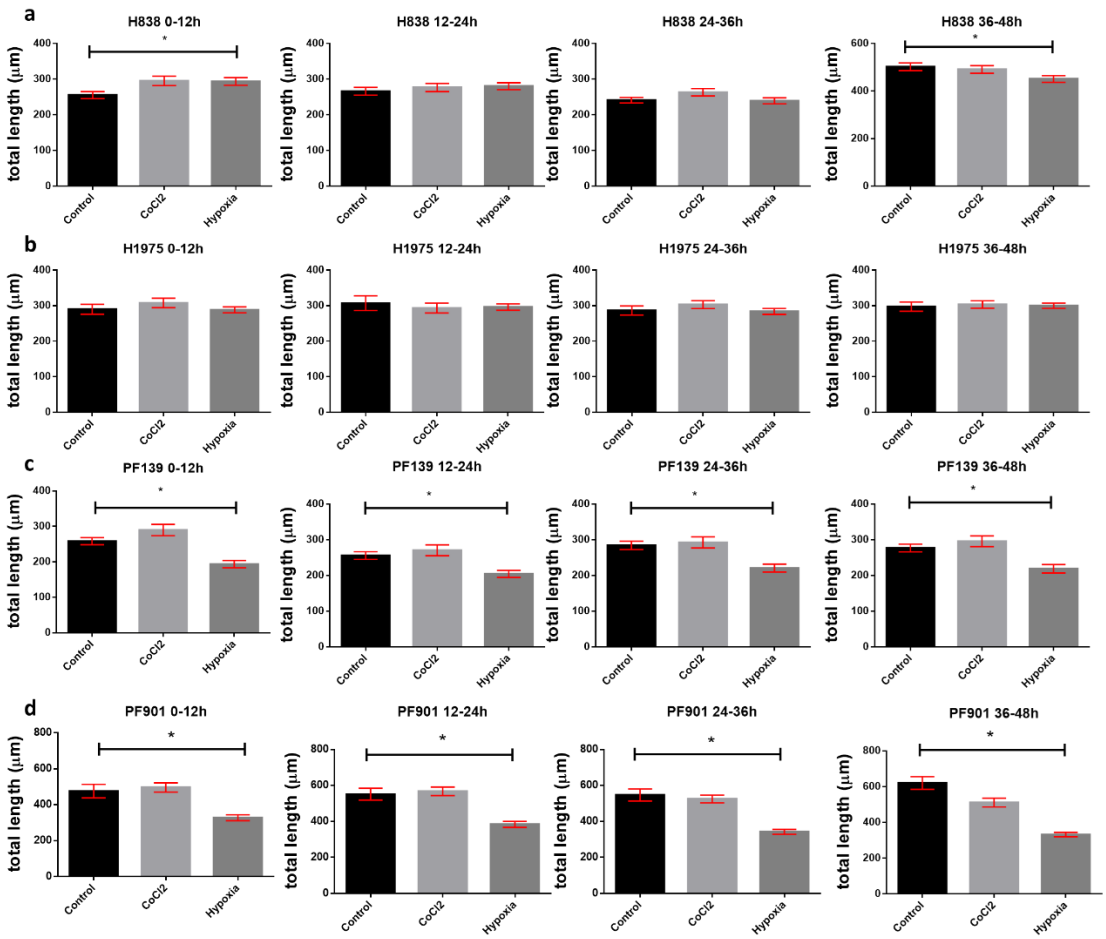

Figure 9. Motility of individual cells in 12-hour intervals of the 48-hour-long exposure to normoxia (21% O_2), 200 µM $CoCl_2$ treatment or hypoxia (1% O_2). Only cells that were presented on the video for the whole period were included in the analysis.

The total length is plotted. Asterisks mark statistically significant differences. Data is derived from three independent experiments. Two independent wells were monitored for each experiment for normoxia and 200 µM $CoCl_2$ treatment, while four independent wells were monitored for hypoxia. Kruskal-Wallis test was used followed by Dunn's multiple comparison post-test. Data plotted as mean +/- SEM. Figure adapted from the author's original publication (63).

4.1.5 Migratory activity under confluent conditions

We found the results based on single-cell motility to be extremely intriguing, however, we were curious whether the presence of cell-cell interactions influences the behavior of the cells. To investigate this, we conducted a wound-healing assay to observe whether hypoxia decreases their movement under confluent conditions. Remarkably, in contrast with the single-cell motility results, hypoxia resulted in significantly faster wound closure for the H838, H1975, and PF901 cell lines compared to normoxic conditions **(Figure 10a)**. In contrast, the PF139 cell line was unable to fully close the wound under hypoxia, whereas it successfully closed the scratch within 60 hours in normal oxygen levels **(Figure 10b)**.

DOI:10.14753/SE.2025.3183

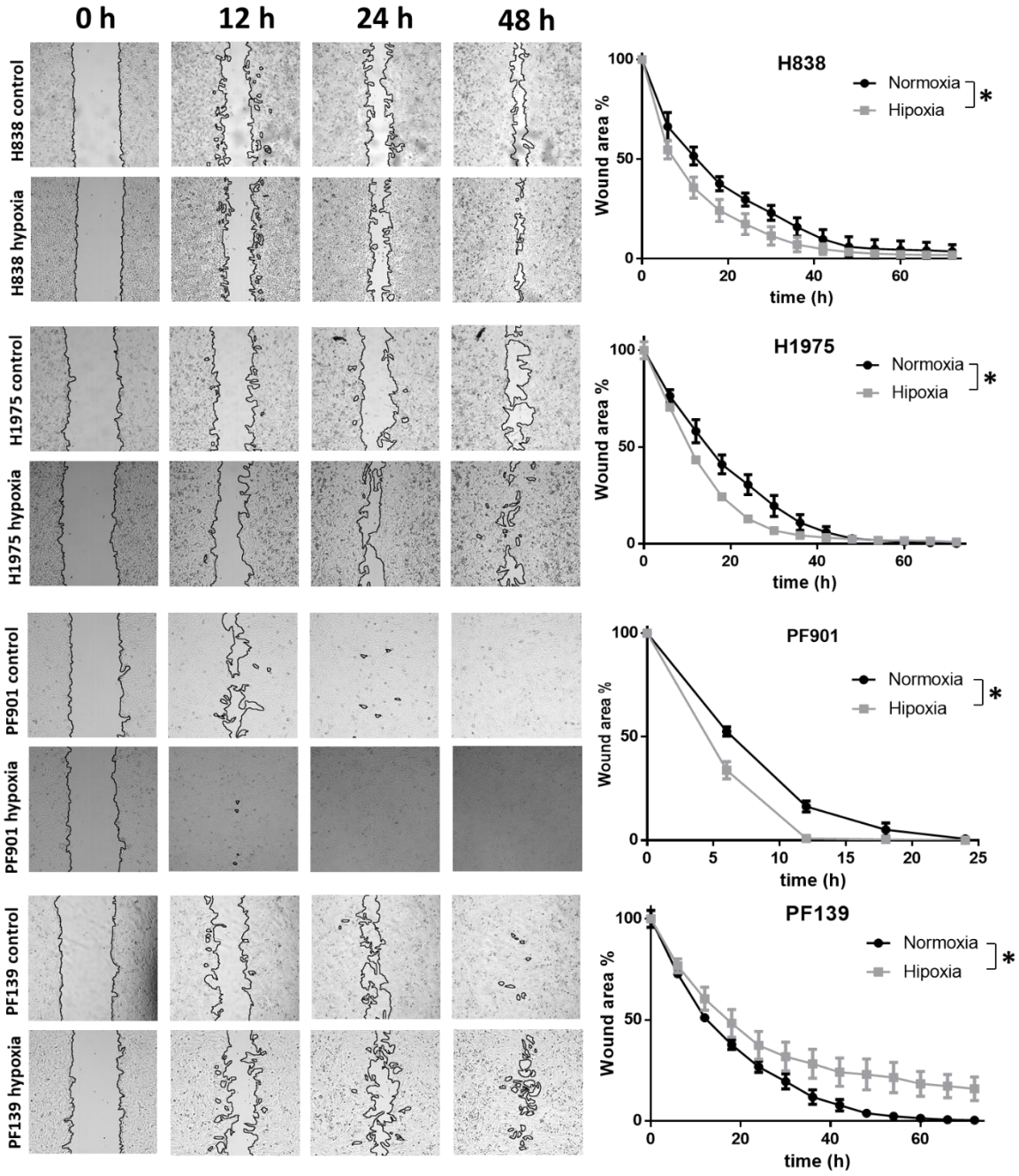

Figure 10. *In vitro* wound healing assay for investigating the effect of hypoxia on four lung adenocarcinoma cell lines migration. a) Representative images illustrating wound closure under both normoxic and hypoxic conditions. b) Graphs show normalized data from the scratch assay experiments. Images were captured every 6 hours over a 72-hour period. Hypoxia resulted in accelerated wound closure for all cell lines, with the exception of PF139**.** Data shown was obtained from three independent experiments, three independent wells were monitored for each experiment. Figure adapted from the author's original publication (63).

DOI:10.14753/SE.2025.3183

4.1.6 Cell line-specific alterations in mRNA expression levels and evaluation of EMT markers in hypoxia

To understand the molecular response to hypoxia on motility we measured the mRNA levels of key EMT markers, namely vimentin, N-cadherin, and E-cadherin, in our panel of lung adenocarcinoma cell lines. Analysis of the basal expression of these genes revealed minor differences in the expression levels of vimentin and E-cadherin between the cell lines. Notably, both PF139 and PF901 showed significantly higher N-cadherin expression compared to H838, which had the lowest baseline motility **(Figure 11a)**. None of the cell lines showed significant changes in the markers studied under hypoxia, however, some variations were observed. In H838, N-cadherin and vimentin levels increased under hypoxic conditions, whereas E-cadherin expression did not change. In H1975, hypoxia slightly increased vimentin expression, with a strong decrease in E-cadherin levels. In PF139, none of the genes were found to be affected by hypoxia. In PF901 cells, hypoxia strongly reduced E-cadherin levels and slightly increased vimentin expression, while N-cadherin levels remained unchanged **(Figure 11b).**

DOI:10.14753/SE.2025.3183

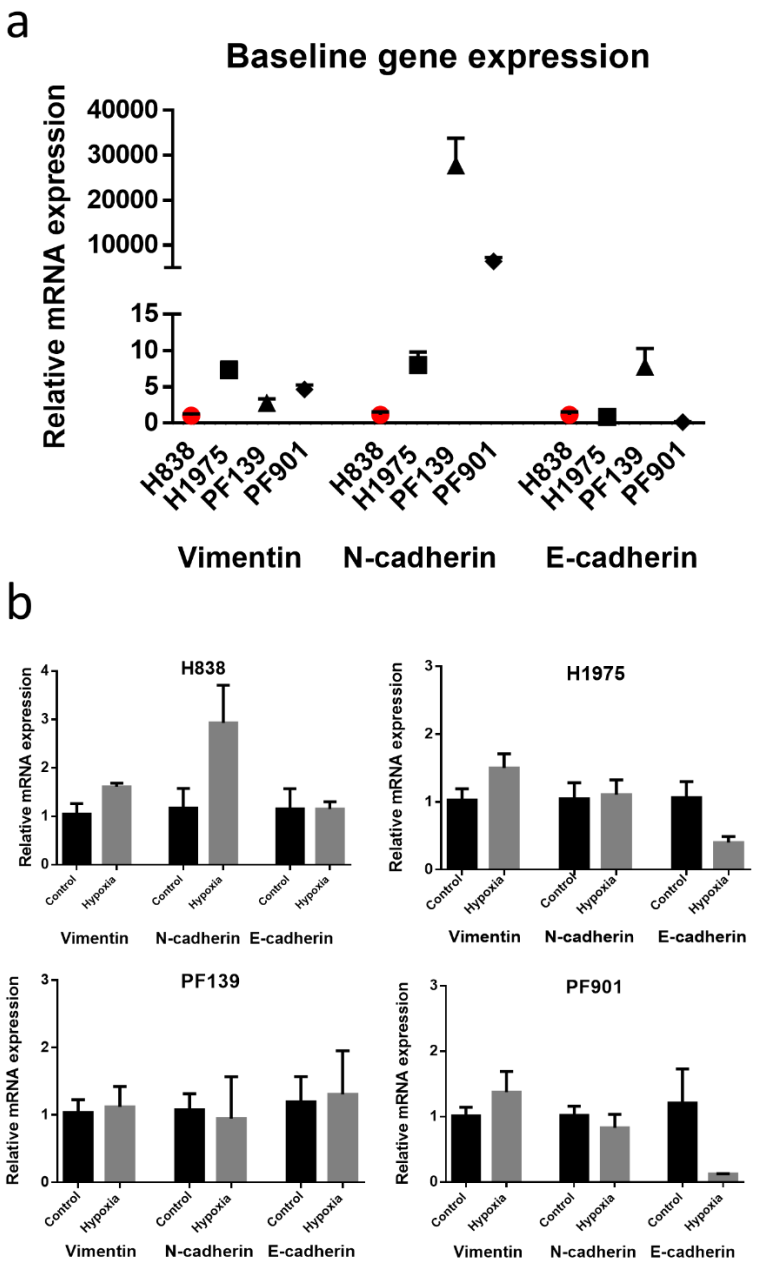

Figure 11. Differences in mRNA expression of genes involved during EMT. a) baseline relative mRNA expression values of vimentin, N-cadherin, E-cadherin. The baseline expression is represented under normoxic conditions normalized to the basal expression of H838 measured by qPCR. The graph shows differences in gene expression levels between the four lung adenocarcinoma cell lines. b) The graphs depict the relative mRNA expression values of vimentin, N-cadherin, and E-cadherin obtained by qPCR. Hypoxia induced cell line-dependent changes. Cells were exposed for 48 hours to normoxic (21% O_2, control) or hypoxic (1 % O_2) conditions. RPLP0 was used as the endogenous control. Data shown was obtained from three independent experiments, plotted as mean ± SEM. Figure adapted from the author's original publication (63).

DOI:10.14753/SE.2025.3183

Although vimentin - a key intermediate filament associated with the mesenchymal phenotype - mRNA levels remained unchanged in response to altered environmental conditions, we investigated whether hypoxia induces changes in the intracellular distribution of the vimentin protein. Immunofluorescence analysis revealed that under normoxic conditions, vimentin showed an uneven distribution, predominantly localized around the nucleus. In contrast, low oxygen concentrations resulted in significant reorganization of vimentin filaments, which adopted a morphology characterized by uniform distribution and alignment with the cell shape **(Figure 12a)**. Quantitative binary mark analysis showed a significant increase in the 2D projection area of vimentin expression under hypoxic conditions. Additionally, analysis of the vimentin signal showed reduced circularity under hypoxia, indicating a transition towards a more mesenchymal-like phenotype **(Figure 12b-c)**.

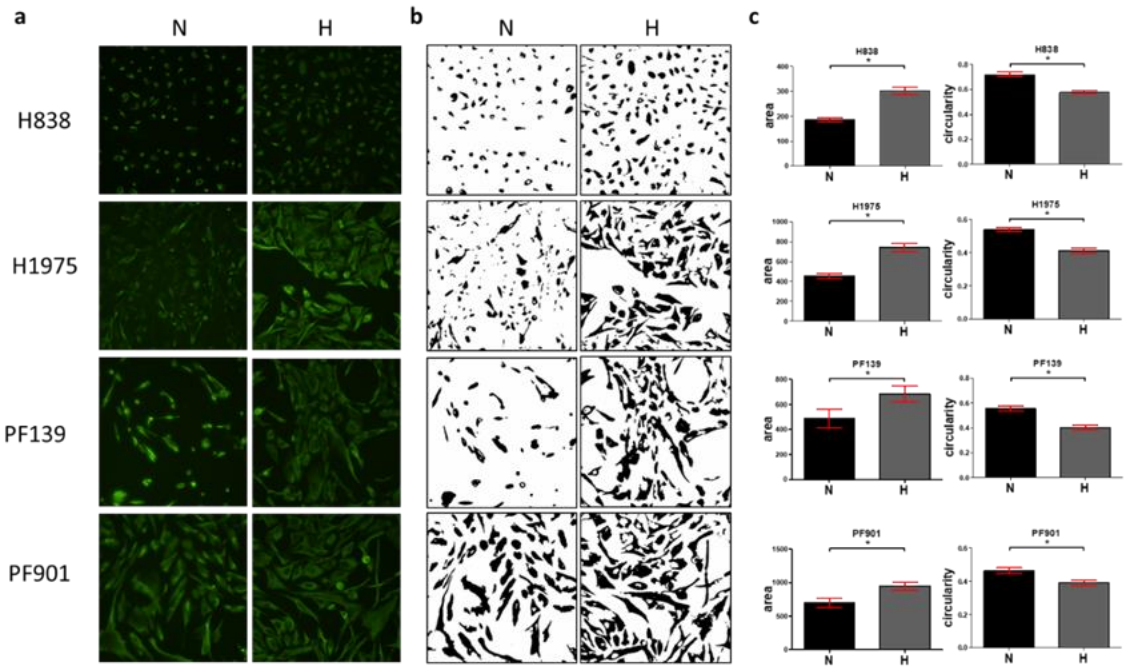

Figure 12. Vimentin expression and morphology under normoxic and hypoxic conditions. a) Representative images of fluorescently labeled vimentin in lung adenocarcinoma cell lines under normoxic (N) and hypoxic (H) conditions. b) Binary masks generated from vimentin expression c) Evaluation of alterations in the area and circularity (shape) of individual cells based on the binary masks. Figure adapted from the author's original publication (63).

DOI:10.14753/SE.2025.3183

4.2 Analysis of resistance mechanisms in vemurafenib-resistant PDTX model

4.2.1 PDTX growth and vemurafenib resistance

To investigate the molecular changes underlying the development of vemurafenib resistance, we established a subcutaneous PDTX model of malignant melanoma and treated with vemurafenib to monitor the acquired drug resistance. Initially, the treatment effectively blocked the tumor growth in the first two generations. However, by the third to sixth generations, resistance had been developed **(Figure 13)**.

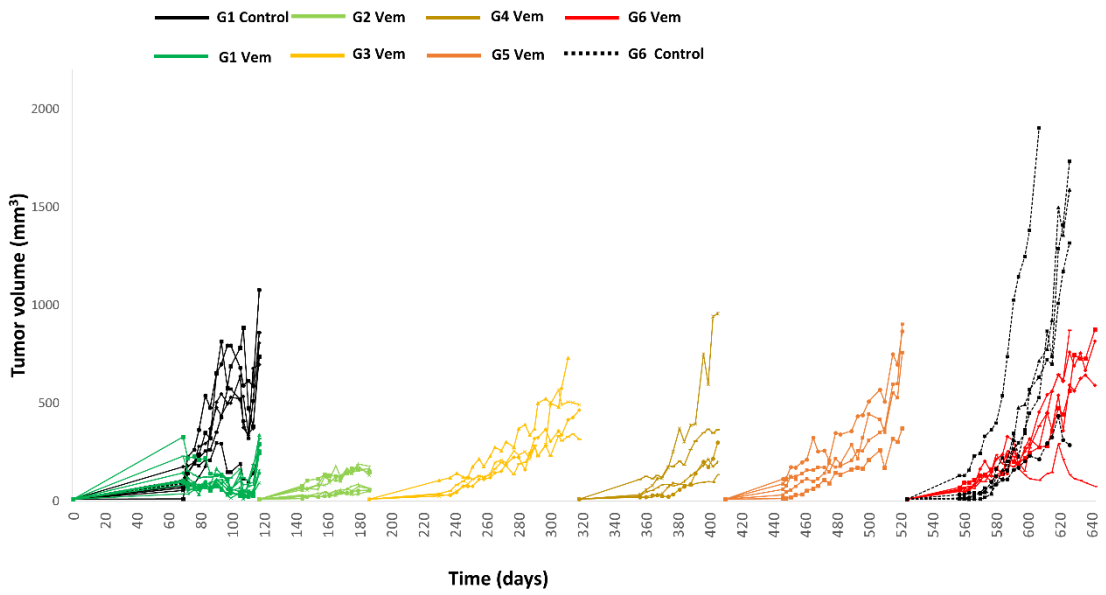

Figure 13. Melanoma PDTX model tumor growth over six mouse generations. In the first generation, two groups were established: one treated with vemurafenib and the other (control group) with water *per os*. To further develop resistance, the treated tumors were serially transplanted (indicated with arrows to note the transition between generations) and sampled. In the sixth generation, a treatment-withdrawal group was started to assess the potential reversal of resistance. Figure adapted from Tóvári, J. et al. (64)

DOI:10.14753/SE.2025.3183

4.2.2 Identification and validation of resistance-associated changes

After the termination of the *in vivo* animal experiment a total of nine samples were sequenced at the mRNA level. These included samples from the control group of the first generation (G1), resistant groups from the third (G3) and fifth generations (G5). Three samples from each group were analyzed, providing a comprehensive overview of the changes that appeared during short- and long-term treatments compared to untreated tumors. The bulk RNA sequencing results revealed a total of 3,991 significant differences between untreated and treated groups, of which 434 were common in the two treated generations. From these, 2 genes were selected for further validation by qPCR, CD27 and IFI27. Both of them have been identified as a prognostic marker, CD27 specifically serves as a prognostic marker in melanoma according to the Protein Atlas database (65). Consistent with the RNA-seq data, CD27 was systematically upregulated while IFI27 was consistently downregulated upon vemurafenib treatment **(Figure 14)**.

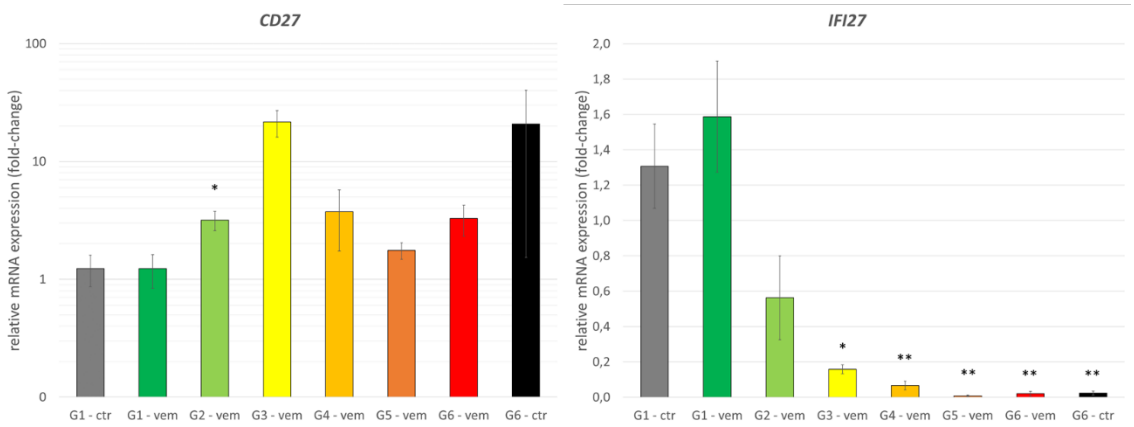

Figure 14. Changes in the relative mRNA expression in melanoma PDTX tissue upon vemurafenib treatment. All data represent relative expression levels normalized to the RPLP0 control. To ensure consistent threshold values for cycle threshold (Ct) determination, all measurements were analyzed within a single study. CD27 was systematically upregulated while IFI27 was downregulated after vemurafenib treatment. *: $p < 0.05$; **: $p < 0.01$. Figure adapted from Tóvári, J. et al. (64)

DOI:10.14753/SE.2025.3183

4.2.3 Immunoblot validation of CD27 and IFI27

For further validation validation, we performed immunoblot analysis of these proteins. The results indicated that CD27 and IFI27 were present in both treatment-naïve (G1) and resistant (G5) samples. However, due to high in-group variance, no relevant changes could be observed **(Figure 15)**.

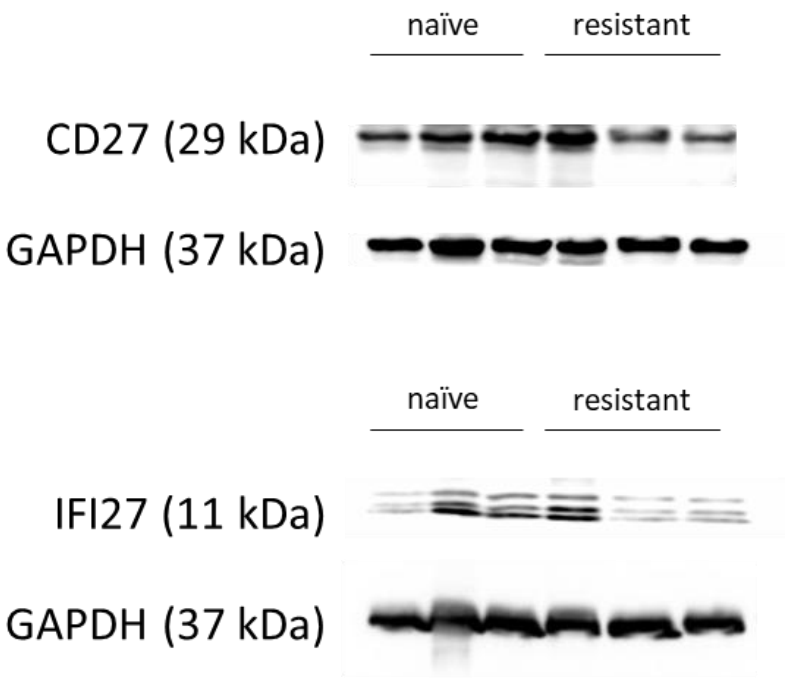

Figure 15. Protein expression patterns upon vemurafenib treatment. Western blot images showing protein level alterations of CD27 and IFI27. Three treatment-naïve (G1) and three treated (G5) animal samples were measured. GAPDH was used as an endogenous control. Figure adapted from Tóvári, J. et al. (64)

4.2.3. Examination of the known resistance mechanisms in the present resistance model

To investigate the mechanisms of vemurafenib resistance in BRAF V600E mutant melanoma PDTX, we aimed to identify potential pathways that contribute to treatment failure. Generally, upon analyzing various signaling pathways in protein level, including the amplification of BRAF and activation of CRAF. However, significant accumulations or activation of these proteins were not detected. There were no changes in the total protein levels of AKT and mTOR, and none of these proteins were found to be

systematically activated, as indicated by the absence of elevated phosphorylated forms. Also, p-MEK 1/2 showed no difference at protein level. ERK 1/2 expression was found elevated in one of the three resistant tumors, however, in-group variance was high, therefore no significant changes could be proved **(Figure 16)**. Surprisingly, PDGFRB, which showed elevated mRNA expression when resistance developed based on RNA sequencing data, had lower protein expression levels **(Figure 16)**. Furthermore, there was no evidence of p53 accumulation, marking increased rate of DNA defects or apoptosis induction **(Figure 16)**.

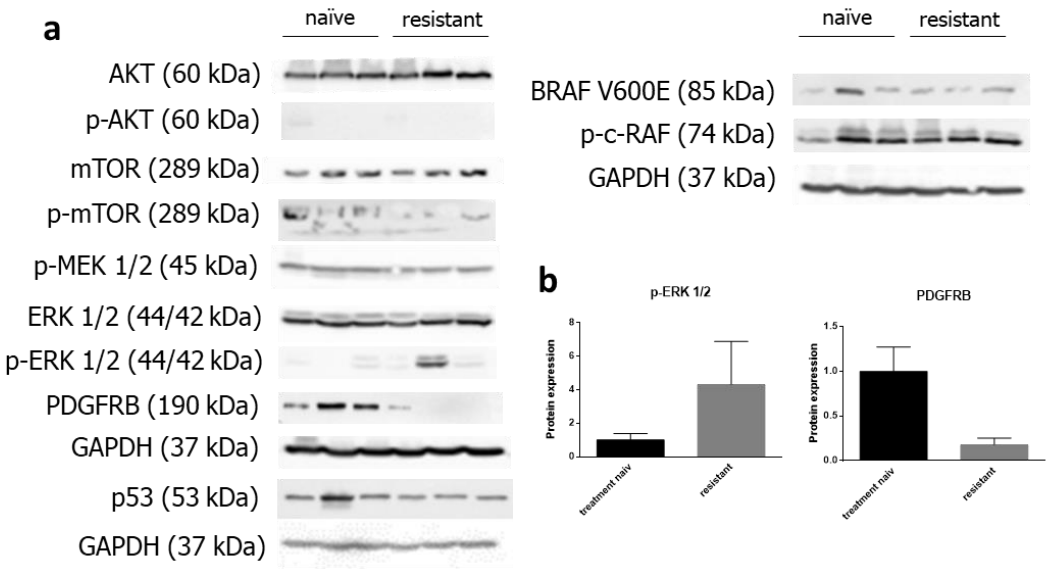

Figure 16. Protein levels and activation of different signaling pathway proteins. a) Representative Western blot images showing AKT, p-AKT, mTOR, p-mTOR, p-MEK 1/2, ERK 1/2, p-ERK 1/2, PDGFRB, BRAF V600E, p-c-RAF and p53 protein levels of the treatment-naïve and the resistant groups. Three treatment-naïve and three treated animal samples (G5) were measured. GAPDH was used as an endogenous control. b) Graph shows the densitometric evaluation of investigated p-ERK 1/2, and PDGFRB protein, normalized to GAPDH and expressed relative to control (treatment-naïve sample). Figure adapted from Tóvári, J. et al. (64)

DOI:10.14753/SE.2025.3183

5. Discussion

To date, lung cancer is recognized as the most lethal form of malignant disease globally, often diagnosed at an advanced metastatic stage, resulting in a poor prognosis. Similarly, malignant melanoma of the skin is characterized by its highly metastatic nature and gives treatment challenges due to its resistance to therapies.

The tumor microenvironment plays a crucial role in cancer development, metastasis and therapy resistance. Metastasis is a process whereby malignant cells migrate from the primary tumor site, infiltrate neighboring tissues, enter the circulatory system and establish secondary tumors in distant organs (13). Therapy resistance can be defined as the ability of cancer cells to tolerate the effects of treatment and reduce or eliminate the therapy's success. Both metastasis and resistance mechanisms are remaining a significant challenge in cancer treatment, making it crucial to understand the underlying processes. Therefore, we studied the migratory activity of lung adenocarcinoma tumor cells under hypoxic conditions to mimic tumor microenvironmental factors and studied the resistance of BRAF V600E mutant melanoma patient-derived tumor xenografts to vemurafenib.

Hypoxia is an environmental condition that is commonly found in tumors due to the unmatured vascularization, characterized by its low oxygen levels. Numerous experimental studies support the role of hypoxia in tumor progression and metastasis formation (37). However, investigating the effects of tumor hypoxia in clinical setting is a challenging process due to tumor heterogeneity. To address this complexity, we investigated cells harboring major mutations that are widely present among LUAD patients, utilizing H1975 (EGFR L858R and T790M), PF901 (BRAF V600E), PF139 (KRAS G12C), and H838 (triple wild type with no known driver mutation) cell lines.

It is well known that hypoxia not only stabilizes the HIF1α protein but also activates the NFκB signaling pathway which contributes to cancer development by stimulating cell proliferation, inhibiting apoptosis and promoting tumor metastasis (66). First, we aimed to observe the cellular adaptation to hypoxia and to investigate whether hypoxia induces apoptosis in the selected panel of lung adenocarcinoma cell lines. Previous research has indicated that increased expression of HIF-1α and HIF-2α in

NSCLC are correlated with an unfavorable prognosis for patients (67,68). However, in certain cancer types, elevated HIF-1α and HIF-2α levels are associated with unexpected tumor suppressive activities (69,70), highlighting context-dependent functions for HIFs (71). The stabilization of HIF occurs in most cases in response to hypoxia, therefore the examination of this protein plays a central role in hypoxia research (72). We observed dramatically high expression of HIF-1α upon hypoxia or hypoxia-mimetic condition induced by $CoCl_2$. Interestingly, $CoCl_2$ induced higher HIF-1α protein levels in all cell lines compared to hypoxia, nevertheless, no equation should be made between real hypoxia and HIF stabilization. In our study, the level of p-NF-κB was slightly decreased probably because HIF-1α can also repress NF-κB-dependent gene expression. This response might be cell-type specific or dependent on the duration of hypoxia. Furthermore, NF-κB is often viewed as a survival-inducing pathway, and the downregulation of this protein suggests that hypoxia appears to be a stressor for LUAD cells at this exposure time (73).

Proliferation and migration of cancer cells are often related processes that can influence each other (74), therefore we examined the changes in the protein levels of the proliferation marker p-Histone H3. Interestingly, we observed a reduction of p-Histone H3 levels in most of the cell lines, suggesting that hypoxia may be a cellular stressor for the cells in this exposure time tested. Meanwhile, no change could be observed in the proliferation rate of tumor cells under hypoxic conditions using a direct viability assay. Our results align with prior studies suggesting that reduced oxygen levels may either decrease (75) or have no impact on the growth rate of various tumor cells (76).

We aimed to investigate the potential changes in the activation of key signaling pathways in response to hypoxic conditions. Recent studies showed that p-FAK-positive patients had a worse prognosis than p-FAK-negative patients in certain cancer types (77, 78), giving high importance to its investigation, since FAK/Src signal transduction pathway may promote the migration and invasion of cancer cells(79,80). We observed limited FAK activation, with only the PF139 cell line showing a response to hypoxia and there was a notable decrease in p-SRC levels in two out of four cell lines. Contrary to some reports (81), we also noted a decrease in P38 pathway activation upon hypoxia. Our results suggested that hypoxic conditions did not enhance the aggressiveness of cancer

cells through these pathways, highlighting the complexity of cellular responses to oxygen deprivation in different cancer cells.

Several studies demonstrated that low oxygen levels have a pro-motility effect on tumor cells. Lehmann and colleagues found that HIF stabilization led to an increased number of metastatic events in an *in vivo* lung colonization model with murine breast cancer (82). Our earlier research revealed that oxygen-deprived conditions heightened the invasive behavior of HT168-M1 melanoma cells, evidenced by their enhanced motility and increased ability to form metastasis (58). Accordingly, we also investigated single-cell motility via time-lapse videomicroscopy. Unexpectedly, 48-hour exposure to hypoxic conditions suppressed single-cell haptotactic motility in three of the four cell lines examined. Current literature on the impact of *in vitro* hypoxia on lung adenocarcinoma cell migration is limited. While studies generally indicate that hypoxia or hypoxia-mimicking agents enhance the migratory capacity of lung tumor cell lines, time-lapse video microscopy has not been used to examine single-cell motility under these conditions. Moreover, the majority of these research has primarily focused on the A549 cell line that exhibit minimal single-cell migration (83). In our study, only the H838 cell line showed enhanced motility under hypoxic conditions during the initial 24-hour period. This observation aligns with a recent publication that revealed increased cellular motility of H838 cells following 24 hours of hypoxia exposure (84).

Since cancer cells may use different strategies for local invasion through different types of migration, we extended our investigation to include migration under confluent conditions using the scratch assay. Interestingly, hypoxia significantly enhanced wound closure in three of the four cell lines, including H838 and PF901, even though their single-cell motility reduced under low oxygen conditions. Investigating the underlying molecular mechanisms, focusing on the alterations in EMT markers might explain these contrasting effects. Our cell panel exhibited notable variations in baseline expression of N-cadherin, with two cell lines showing significantly increased levels compared to H838. N-cadherin overexpression correlates with a more aggressive tumor phenotype (85) and reduced overall survival in patients with non-small cell lung cancer (86). Although we observed changes in the EMT markers upon hypoxia which are correlated to the metastasis-promoting effects of hypoxia - decreased E-cadherin expression in PF901 and H1975 cell lines and increased N-cadherin expression in H838 - the differences were not

enough to make robust conclusions. Therefore, we investigated the vimentin protein using immunofluorescent staining. Our analysis revealed that hypoxia significantly changed vimentin morphology. Under normoxic conditions, vimentin showed uneven, varying distribution within cell boundaries often localized near the nucleus. In contrast, hypoxic exposure led to a more homogenic, filamentous distribution across all cell lines, showing a more mesenchymal-like morphology. These changes are similar to a previous study where Maier and colleagues observed similar morphological changes in vimentin upon EMT induction by TGF-β treatment (87).

To further explore the challenges of treating patients, we established a PDTX model from a melanoma patient harboring BRAF V600E mutation to investigate potential resistance-relevant mechanisms and markers. This model has significant intratumoral heterogeneity and preserve key microenvironmental features, mimicking the complexity of human solid tumors. During the treatment, vemurafenib effectively blocked the tumor growth for more than two months. However, by the third to sixth generations, resistance had developed, indicating the tumor's adaptation to the therapy. This observation aligns with the clinical data on acquired resistance to BRAF inhibitors in melanoma patients (88).

To elucidate the underlying mechanisms of resistance, we performed a bulk RNA sequencing of the PDTX models at different stages of treatment, to identify differences after short- and long-term vemurafenib treatment. From the numerous gene expression differences observed, we selected two genes for qPCR validation. CD27, which showed increased expression, and IFI27, which exhibited decreased expression at the RNA levels. These genes were chosen based on their previously reported prognostic value in cancer patients (89). We observed a systematic upregulation of CD27, while IFI27 showed a strong and consistent downregulation, which can suggest their roles in the development of vemurafenib resistance in our PDTX model. Further validation by immunoblot analysis revealed the presence of CD27 and IFI27 in both treatment-naïve (G1) and resistant (G5) samples with no consistent differences. CD27 is expressed on the surface of immune cells, including activated T and B cells, as well as NK cells. Given that NOD-SCID mice have diminished T and B cell functions, we hypothesize that NK cell infiltration might be responsible for the phenomenon, since this model does not completely lack NK cells (90). Different studies revealed that the role of IFI27 in cancer progression is context-

dependent. In esophageal cancer, stabilization of IFI27 mRNA promotes tumor progression and angiogenesis (91). Conversely, in breast cancer metastases, IFI27 showed systematic downregulation (92). These contrasting findings highlight the complexity of IFI27 and warrants further specific investigation to reveal its possible therapeutic values.

Furthermore, in our investigation of vemurafenib resistance mechanisms, we sought to identify changes in cellular signaling pathways that can contribute to treatment failure. Surprisingly, our findings diverged from commonly reported resistance mechanisms observed in similar studies (93). We found no evidence of BRAF or CRAF activation, increased PDGFR expression, enhanced AKT-mTOR signaling, or alterations in MAP2K2 (MEK 1/2) andP44/42 (ERK 1/2) expression or phosphorylation levels. The persistent ERK 1/2 activation observed in one of the resistant tumors indicates that BRAFi therapy had lost its efficacy in suppressing the primary proliferative pathway, as proved in the clinical practice (94).

DOI:10.14753/SE.2025.3183

6. Conclusion

In this study, we aimed to determine the role of hypoxia on the motility of lung adenocarcinoma cell lines and the acquired resistance mechanisms of a vemurafenib-resistant patient-derived tumor xenograft PDTX model. Our findings indicate that:

- (1) Hypoxic conditions lowered the activation level of SRC, P38 of FAK pathways in the LUAD cell lines as well as the level of proliferation marker phospho-Histone H3, indicating that it may act as a cellular stressor for this time exposure.
- (2) 48-hour exposure to hypoxic conditions suppressed single-cell motility in three of the four cell lines, however invasion under confluent conditions was enhanced upon hypoxia for most of the cell lines.
- (2) $CoCl_2$ failed to replicate the effects of true hypoxic conditions on single-cell motility, warranting caution in the interpretation of hypoxic studies solely based on the use of this hypoxia-mimicking agent.
- (2) Changes in the EMT markers are consistent with enhanced motility and metastasis-promoting effect of hypoxia.
- (3) The established PDTX model of melanoma developed resistance to vemurafenib.
- (4) We identified new potential markers of resistance at RNA level, however, failed to validate them on the protein level.
- (4) Resistant tumors exhibited different resistant mechanisms from the reactivation of RAF/MEK/ERK pathway reported in the literature.

DOI:10.14753/SE.2025.3183

7. Summary

We investigated two critical aspects of cancer biology. The effects of hypoxia on lung adenocarcinoma cell motility as referred to the metastasis formation and the mechanisms of acquired resistance to BRAF inhibitors in melanoma. Regarding hypoxia, we observed cell-line-specific and time-dependent effects on the migratory activity of the lung adenocarcinoma cells. Notably, hypoxia either maintained or slightly reduced cellular proliferation. Interestingly, the hypoxia-mimicking agent $CoCl_2$ failed to replicate the effects of true hypoxic conditions on single-cell motility. We found that invasion under confluent conditions was enhanced upon hypoxia for most of the cell lines, even in cell lines showing reduced single-cell motility. These changes aligned with alterations in EMT markers. While the exact mechanism underlying the differential effects of hypoxia on single-cell motility and wound closure remains to be fully elucidated, we suspect that distinct patterns of cell-cell and cell-ECM contacts play a crucial role, possibly by modulating the complete or partial transition from epithelial to mesenchymal phenotype. Our study provides valuable insights into hypoxia- and HIF-related responses in various lung adenocarcinoma models, in terms of motility, proliferation, and apoptotic activity. The high variance in cellular responses to hypoxia presents a significant challenge in cancer treatment, possibly contributing to the clinical failure of HIF inhibitors. Further investigations are necessary to gain a more comprehensive understanding of how hypoxia influences cancer progression across different tumor types and microenvironmental factors. Next, in an attempt to model therapeutic resistance, we established a PDTX model of melanoma that developed resistance to vemurafenib, closely mimicking the acquired resistance observed in clinical settings. This model provides a valuable platform for investigating the mechanisms underlying BRAF inhibitor resistance in melanoma. Through comprehensive transcriptomic analysis, we identified potential resistance markers, including CD27 and IFI27, which showed distinct expression patterns across treatment stages. However, we failed to validate them on the protein level. Notably, our resistant tumors did not exhibit commonly reported resistance mechanisms, such as BRAF/CRAF activation or enhanced AKT-mTOR signaling possibly mirroring RAF/MEK/ERK pathway-independent resistance mechanisms.

8. References

1. Bray F, Laversanne M, Sung H, Ferlay J, Siegel RL, Soerjomataram I, et al. Global cancer statistics 2022: GLOBOCAN estimates of incidence and mortality worldwide for 36 cancers in 185 countries. CA Cancer J Clin. 2024;74(3):229-63.
2. Molina JR, Yang P, Cassivi SD, Schild SE, Adjei AA. Non-small cell lung cancer: epidemiology, risk factors, treatment, and survivorship. Mayo Clin Proc. 2008;83(5):584-94.
3. Zarogoulidis P, Matthaios D, Kosmidis C, Hohenforst-Schmidt W, Tsakiridis K, Mpaka S, et al. Effective early diagnosis for NSCLC: an algorithm. Expert Rev Respir Med. 2021;15(11):1437-45.
4. https://stat.nrr.hu/. 2024.11.13.
5. Kenessey I, Parrag P, Dobozi M, Szatmari I, Weber A, Nagy P, et al. The epidemiology of lung cancer in Hungary based on the characteristics of patients diagnosed in 2018. Sci Rep. 2024;14(1):20064.
6. Parrag P, Weber A, Liszkay G, Nagy P, Kasler M, Polgar C, et al. [Hungarian situation of melanoma incidence and mortality in the first two decades of 21st century]. Magy Onkol. 2022;66(2):94-9.
7. Lantuejoul S, Sound-Tsao M, Cooper WA, Girard N, Hirsch FR, Roden AC, et al. PD-L1 Testing for Lung Cancer in 2019: Perspective From the IASLC Pathology Committee. J Thorac Oncol. 2020;15(4):499-519.
8. https://emedicine.medscape.com/article/279960-treatment#. 2024.11.19.
9. Mina SA, Shanshal M, Leventakos K, Parikh K. Emerging Targeted Therapies in Non-Small-Cell Lung Cancer (NSCLC). Cancers (Basel). 2025;17(3).
10. https://emedicine.medscape.com/article/280245-overview?form=fpf. 2024.11.19.
11. Boutros A, Croce E, Ferrari M, Gili R, Massaro G, Marconcini R, et al. The treatment of advanced melanoma: Current approaches and new challenges. Crit Rev Oncol Hematol. 2024;196:104276.
12. Nichols L, Saunders R, Knollmann FD. Causes of death of patients with lung cancer. Arch Pathol Lab Med. 2012;136(12):1552-7.
13. Massague J, Obenauf AC. Metastatic colonization by circulating tumour cells. Nature. 2016;529(7586):298-306.

14. Luzzi KJ, MacDonald IC, Schmidt EE, Kerkvliet N, Morris VL, Chambers AF, et al. Multistep nature of metastatic inefficiency: dormancy of solitary cells after successful extravasation and limited survival of early micrometastases. Am J Pathol. 1998;153(3):865-73.
15. He J, Xiong L, Li Q, Lin L, Miao X, Yan S, et al. 3D modeling of cancer stem cell niche. Oncotarget. 2018;9(1):1326-45.
16. Vasan N, Baselga J, Hyman DM. A view on drug resistance in cancer. Nature. 2019;575(7782):299-309.
17. Turajlic S, Furney SJ, Stamp G, Rana S, Ricken G, Oduko Y, et al. Whole-genome sequencing reveals complex mechanisms of intrinsic resistance to BRAF inhibition. Ann Oncol. 2014;25(5):959-67.
18. Lei ZN, Tian Q, Teng QX, Wurpel JND, Zeng L, Pan Y, et al. Understanding and targeting resistance mechanisms in cancer. MedComm (2020). 2023;4(3):e265.
19. Wicki A, Mandala M, Massi D, Taverna D, Tang H, Hemmings BA, et al. Acquired Resistance to Clinical Cancer Therapy: A Twist in Physiological Signaling. Physiol Rev. 2016;96(3):805-29.
20. Hu X, Zhang Z. Understanding the Genetic Mechanisms of Cancer Drug Resistance Using Genomic Approaches. Trends Genet. 2016;32(2):127-37.
21. Kara A, Ozgur A, Nalbantoglu S, Karadag A. DNA repair pathways and their roles in drug resistance for lung adenocarcinoma. Mol Biol Rep. 2021;48(4):3813-25.
22. Davies H, Bignell GR, Cox C, Stephens P, Edkins S, Clegg S, et al. Mutations of the BRAF gene in human cancer. Nature. 2002;417(6892):949-54.
23. Timar J, Ladanyi A. Molecular Pathology of Skin Melanoma: Epidemiology, Differential Diagnostics, Prognosis and Therapy Prediction. Int J Mol Sci. 2022;23(10).
24. Pollock PM, Meltzer PS. A genome-based strategy uncovers frequent BRAF mutations in melanoma. Cancer Cell. 2002;2(1):5-7.
25. Flaherty KT, Yasothan U, Kirkpatrick P. Vemurafenib. Nat Rev Drug Discov. 2011;10(11):811-2.
26. Larkin J, Ascierto PA, Dreno B, Atkinson V, Liszkay G, Maio M, et al. Combined vemurafenib and cobimetinib in BRAF-mutated melanoma. N Engl J Med. 2014;371(20):1867-76.

27. Robert C, Karaszewska B, Schachter J, Rutkowski P, Mackiewicz A, Stroiakovski D, et al. Improved overall survival in melanoma with combined dabrafenib and trametinib. N Engl J Med. 2015;372(1):30-9.
28. Bollag G, Tsai J, Zhang J, Zhang C, Ibrahim P, Nolop K, et al. Vemurafenib: the first drug approved for BRAF-mutant cancer. Nat Rev Drug Discov. 2012;11(11):873-86.
29. Subbiah V, Baik C, Kirkwood JM. Clinical Development of BRAF plus MEK Inhibitor Combinations. Trends Cancer. 2020;6(9):797-810.
30. Brummer C, Faerber S, Bruss C, Blank C, Lacroix R, Haferkamp S, et al. Metabolic targeting synergizes with MAPK inhibition and delays drug resistance in melanoma. Cancer Lett. 2019;442:453-63.
31. Botton T, Talevich E, Mishra VK, Zhang T, Shain AH, Berquet C, et al. Genetic Heterogeneity of BRAF Fusion Kinases in Melanoma Affects Drug Responses. Cell Rep. 2019;29(3):573-88 e7.
32. Ades F, Metzger-Filho O. Targeting the Cellular Signaling: BRAF Inhibition and Beyond for the Treatment of Metastatic Malignant Melanoma. Dermatol Res Pract. 2012;2012:259170.
33. Liu Y, Wu W, Cai C, Zhang H, Shen H, Han Y. Patient-derived xenograft models in cancer therapy: technologies and applications. Signal Transduct Target Ther. 2023;8(1):160.
34. Kemper K, Krijgsman O, Kong X, Cornelissen-Steijger P, Shahrabi A, Weeber F, et al. BRAF(V600E) Kinase Domain Duplication Identified in Therapy-Refractory Melanoma Patient-Derived Xenografts. Cell Rep. 2016;16(1):263-77.
35. Kurose K, Hoshaw-Woodard S, Adeyinka A, Lemeshow S, Watson PH, Eng C. Genetic model of multi-step breast carcinogenesis involving the epithelium and stroma: clues to tumour-microenvironment interactions. Hum Mol Genet. 2001;10(18):1907-13.
36. Fearon ER, Vogelstein B. A genetic model for colorectal tumorigenesis. Cell. 1990;61(5):759-67.
37. Hanahan D, Weinberg RA. Hallmarks of cancer: the next generation. Cell. 2011;144(5):646-74.

38. Muz B, de la Puente P, Azab F, Azab AK. The role of hypoxia in cancer progression, angiogenesis, metastasis, and resistance to therapy. Hypoxia (Auckl). 2015;3:83-92.
39. McKeown SR. Defining normoxia, physoxia and hypoxia in tumours-implications for treatment response. Br J Radiol. 2014;87(1035):20130676.
40. Le QT, Chen E, Salim A, Cao H, Kong CS, Whyte R, et al. An evaluation of tumor oxygenation and gene expression in patients with early stage non-small cell lung cancers. Clin Cancer Res. 2006;12(5):1507-14.
41. Saxena K, Jolly MK. Acute vs. Chronic vs. Cyclic Hypoxia: Their Differential Dynamics, Molecular Mechanisms, and Effects on Tumor Progression. Biomolecules. 2019;9(8).
42. Liu Q, Palmgren VAC, Danen EH, Le Devedec SE. Acute vs. chronic vs. intermittent hypoxia in breast Cancer: a review on its application in in vitro research. Mol Biol Rep. 2022;49(11):10961-73.
43. Semenza GL, Wang GL. A nuclear factor induced by hypoxia via de novo protein synthesis binds to the human erythropoietin gene enhancer at a site required for transcriptional activation. Mol Cell Biol. 1992;12(12):5447-54.
44. Maxwell PH, Wiesener MS, Chang GW, Clifford SC, Vaux EC, Cockman ME, et al. The tumour suppressor protein VHL targets hypoxia-inducible factors for oxygen-dependent proteolysis. Nature. 1999;399(6733):271-5.
45. Al Tameemi W, Dale TP, Al-Jumaily RMK, Forsyth NR. Hypoxia-Modified Cancer Cell Metabolism. Front Cell Dev Biol. 2019;7:4.
46. Berchner-Pfannschmidt U, Frede S, Wotzlaw C, Fandrey J. Imaging of the hypoxia-inducible factor pathway: insights into oxygen sensing. Eur Respir J. 2008;32(1):210-7.
47. Mole DR, Blancher C, Copley RR, Pollard PJ, Gleadle JM, Ragoussis J, et al. Genome-wide association of hypoxia-inducible factor (HIF)-1alpha and HIF-2alpha DNA binding with expression profiling of hypoxia-inducible transcripts. J Biol Chem. 2009;284(25):16767-75.
48. Semenza GL. Hypoxia-inducible factor 1 (HIF-1) pathway. Sci STKE. 2007;2007(407):cm8.

49. Svajda L, Randelovic I, Surguta SE, Baranyi M, Cserepes M, Tovari J. Targeting hypoxia in combination with paclitaxel to enhance therapeutic efficacy in breast and ovarian cancer. Biomed Pharmacother. 2024;180:117601.
50. Melvin A, Mudie S, Rocha S. Further insights into the mechanism of hypoxia-induced NFkappaB. [corrected]. Cell Cycle. 2011;10(6):879-82.
51. D'Ignazio L, Rocha S. Hypoxia Induced NF-kappaB. Cells. 2016;5(1).
52. Nieto MA, Huang RY, Jackson RA, Thiery JP. Emt: 2016. Cell. 2016;166(1):21-45.
53. Tirpe AA, Gulei D, Ciortea SM, Crivii C, Berindan-Neagoe I. Hypoxia: Overview on Hypoxia-Mediated Mechanisms with a Focus on the Role of HIF Genes. Int J Mol Sci. 2019;20(24).
54. Lamouille S, Xu J, Derynck R. Molecular mechanisms of epithelial-mesenchymal transition. Nat Rev Mol Cell Biol. 2014;15(3):178-96.
55. Thiery JP. Epithelial-mesenchymal transitions in tumour progression. Nat Rev Cancer. 2002;2(6):442-54.
56. Friedl P, Wolf K. Tumour-cell invasion and migration: diversity and escape mechanisms. Nat Rev Cancer. 2003;3(5):362-74.
57. Polacheck WJ, Zervantonakis IK, Kamm RD. Tumor cell migration in complex microenvironments. Cell Mol Life Sci. 2013;70(8):1335-56.
58. Tatrai E, Bartal A, Gacs A, Paku S, Kenessey I, Garay T, et al. Cell type-dependent HIF1 alpha-mediated effects of hypoxia on proliferation, migration and metastatic potential of human tumor cells. Oncotarget. 2017;8(27):44498-510.
59. Hegedus L, Rittler D, Garay T, Stockhammer P, Kovacs I, Dome B, et al. HDAC Inhibition Induces PD-L1 Expression in a Novel Anaplastic Thyroid Cancer Cell Line. Pathol Oncol Res. 2020;26(4):2523-35.
60. Baranyi M, Molnar E, Hegedus L, Gabriel Z, Petenyi FG, Bordas F, et al. Farnesyl-transferase inhibitors show synergistic anticancer effects in combination with novel KRAS-G12C inhibitors. Br J Cancer. 2024.
61. Piccinini F, Kiss A, Horvath P. CellTracker (not only) for dummies. Bioinformatics. 2016;32(6):955-7.

62. Suarez-Arnedo A, Torres Figueroa F, Clavijo C, Arbelaez P, Cruz JC, Munoz-Camargo C. An image J plugin for the high throughput image analysis of in vitro scratch wound healing assays. PLoS One. 2020;15(7):e0232565.
63. Surguta SE, Baranyi M, Svajda L, Cserepes M, Randelovic I, Tatrai E, et al. Differential effects of hypoxia on motility using various in vitro models of lung adenocarcinoma. Sci Rep. 2024;14(1):20482.
64. Tovari J, Vari-Mezo D, Surguta SE, Ladanyi A, Kigyos A, Cserepes M. Evolving Acquired Vemurafenib Resistance in a BRAF V600E Mutant Melanoma PDTX Model to Reveal New Potential Targets. Cells. 2023;12(14).
65. https://www.proteinatlas.org/. 2024.11.21.
66. Xia Y, Shen S, Verma IM. NF-kappaB, an active player in human cancers. Cancer Immunol Res. 2014;2(9):823-30.
67. Giatromanolaki A, Koukourakis MI, Sivridis E, Turley H, Talks K, Pezzella F, et al. Relation of hypoxia inducible factor 1 alpha and 2 alpha in operable non-small cell lung cancer to angiogenic/molecular profile of tumours and survival. Br J Cancer. 2001;85(6):881-90.
68. Wu XH, Qian C, Yuan K. Correlations of hypoxia-inducible factor-1alpha/hypoxia-inducible factor-2alpha expression with angiogenesis factors expression and prognosis in non-small cell lung cancer. Chin Med J (Engl). 2011;124(1):11-8.
69. Acker T, Diez-Juan A, Aragones J, Tjwa M, Brusselmans K, Moons L, et al. Genetic evidence for a tumor suppressor role of HIF-2alpha. Cancer Cell. 2005;8(2):131-41.
70. Mazumdar J, Hickey MM, Pant DK, Durham AC, Sweet-Cordero A, Vachani A, et al. HIF-2alpha deletion promotes Kras-driven lung tumor development. Proc Natl Acad Sci U S A. 2010;107(32):14182-7.
71. Keith B, Johnson RS, Simon MC. HIF1alpha and HIF2alpha: sibling rivalry in hypoxic tumour growth and progression. Nat Rev Cancer. 2011;12(1):9-22.
72. Semenza GL. Hypoxia, clonal selection, and the role of HIF-1 in tumor progression. Crit Rev Biochem Mol Biol. 2000;35(2):71-103.

73. Bandarra D, Biddlestone J, Mudie S, Muller HA, Rocha S. HIF-1alpha restricts NF-kappaB-dependent gene expression to control innate immunity signals. Dis Model Mech. 2015;8(2):169-81.
74. Gallaher JA, Brown JS, Anderson ARA. The impact of proliferation-migration tradeoffs on phenotypic evolution in cancer. Sci Rep. 2019;9(1):2425.
75. Nisar H, Sanchidrian Gonzalez PM, Brauny M, Labonte FM, Schmitz C, Roggan MD, et al. Hypoxia Changes Energy Metabolism and Growth Rate in Non-Small Cell Lung Cancer Cells. Cancers (Basel). 2023;15(9).
76. Wang X, Schneider A. HIF-2alpha-mediated activation of the epidermal growth factor receptor potentiates head and neck cancer cell migration in response to hypoxia. Carcinogenesis. 2010;31(7):1202-10.
77. Peng K, Li S, Li Q, Zhang C, Yuan Y, Liu M, et al. Positive Phospho-Focal Adhesion Kinase in Gastric Cancer Associates With Poor Prognosis After Curative Resection. Front Oncol. 2022;12:953938.
78. Yu G, Xu M, Zhou L, Zheng K, Zhu X, Sui J, et al. High expression of phosphorylated focal adhesion kinase predicts a poor prognosis in human colorectal cancer. Front Pharmacol. 2022;13:989999.
79. Bae IH, Yoon SH, Lee SB, Park JK, Ho JN, Um HD. Signaling components involved in Bcl-w-induced migration of gastric cancer cells. Cancer Lett. 2009;277(1):22-8.
80. Slack JK, Adams RB, Rovin JD, Bissonette EA, Stoker CE, Parsons JT. Alterations in the focal adhesion kinase/Src signal transduction pathway correlate with increased migratory capacity of prostate carcinoma cells. Oncogene. 2001;20(10):1152-63.
81. Xu L, Pathak PS, Fukumura D. Hypoxia-induced activation of p38 mitogen-activated protein kinase and phosphatidylinositol 3'-kinase signaling pathways contributes to expression of interleukin 8 in human ovarian carcinoma cells. Clin Cancer Res. 2004;10(2):701-7.
82. Lehmann S, Te Boekhorst V, Odenthal J, Bianchi R, van Helvert S, Ikenberg K, et al. Hypoxia Induces a HIF-1-Dependent Transition from Collective-to-Amoeboid Dissemination in Epithelial Cancer Cells. Curr Biol. 2017;27(3):392-400.

83. Wang T, Niki T, Goto A, Ota S, Morikawa T, Nakamura Y, et al. Hypoxia increases the motility of lung adenocarcinoma cell line A549 via activation of the epidermal growth factor receptor pathway. Cancer Sci. 2007;98(4):506-11.
84. Yan F, Teng Y, Li X, Zhong Y, Li C, Yan F, et al. Hypoxia promotes non-small cell lung cancer cell stemness, migration, and invasion via promoting glycolysis by lactylation of SOX9. Cancer Biol Ther. 2024;25(1):2304161.
85. Mrozik KM, Blaschuk OW, Cheong CM, Zannettino ACW, Vandyke K. N-cadherin in cancer metastasis, its emerging role in haematological malignancies and potential as a therapeutic target in cancer. BMC Cancer. 2018;18(1):939.
86. Hui L, Zhang S, Dong X, Tian D, Cui Z, Qiu X. Prognostic significance of twist and N-cadherin expression in NSCLC. PLoS One. 2013;8(4):e62171.
87. Maier J, Traenkle B, Rothbauer U. Real-time analysis of epithelial-mesenchymal transition using fluorescent single-domain antibodies. Sci Rep. 2015;5:13402.
88. Sullivan RJ, Flaherty KT. Resistance to BRAF-targeted therapy in melanoma. Eur J Cancer. 2013;49(6):1297-304.
89. Wang Y, Guan L, Zhao Y, Yang Y, Wang Y, Feng S, et al. A Comprehensive Pan-cancer Analysis of the Biological Immunomodulatory Function and Clinical Value of CD27. J Cancer. 2024;15(2):508-25.
90. Miao M, Masengere H, Yu G, Shan F. Reevaluation of NOD/SCID Mice as NK Cell-Deficient Models. Biomed Res Int. 2021;2021:8851986.
91. Zhang Y, Chen C, Liu Z, Guo H, Lu W, Hu W, et al. PABPC1-induced stabilization of IFI27 mRNA promotes angiogenesis and malignant progression in esophageal squamous cell carcinoma through exosomal miRNA-21-5p. J Exp Clin Cancer Res. 2022;41(1):111.
92. Szekely B, Bossuyt V, Li X, Wali VB, Patwardhan GA, Frederick C, et al. Immunological differences between primary and metastatic breast cancer. Ann Oncol. 2018;29(11):2232-9.
93. Proietti I, Skroza N, Bernardini N, Tolino E, Balduzzi V, Marchesiello A, et al. Mechanisms of Acquired BRAF Inhibitor Resistance in Melanoma: A Systematic Review. Cancers (Basel). 2020;12(10).

DOI:10.14753/SE.2025.3183

94. Das Thakur M, Salangsang F, Landman AS, Sellers WR, Pryer NK, Levesque MP, et al. Modelling vemurafenib resistance in melanoma reveals a strategy to forestall drug resistance. Nature. 2013;494(7436):251-5.

9. Bibliography of the candidate's publications

Articles related to the thesis:

1. **Surguta, S.E.,** Baranyi, M., Svajda, L. et al. Differential effects of hypoxia on motility using various in vitro models of lung adenocarcinoma. Sci Rep 14, 20482 (2024). **IF: 3.8**

2. Tovari, J., Vari-Mezo, D., **Surguta, S.E**., Ladanyi, A., Kigyos, A., Cserepes, M. Evolving Acquired Vemurafenib Resistance in a BRAF V600E Mutant Melanoma PDTX Model to Reveal New Potential Targets. Cells 12, 1919 (2023). **IF: 5.1**

Articles not related to the thesis:

3. Faragó A, Zvara Á, Tiszlavicz L, Hunyadi-Gulyás É, Darula Z, Hegedűs Z, Szabó E, **Surguta, S.E,** Tóvári J, Puskás LG, Szebeni GJ. Lectin-Based Immunophenotyping and Whole Proteomic Profiling of CT-26 Colon Carcinoma Murine Model. Int J Mol Sci. 2024 Apr 4;25(7):4022. **IF: 4.9**

4. Tátrai, E, Ranđelović, I, **Surguta, S.E,** Tóvári, J. Role of Hypoxia and Rac1 Inhibition in the Metastatic Cascade. Cancers (Basel). 2024 May 14;16(10):1872. **IF: 4.5**

5. Svajda, L, Ranđelović, I, **Surguta, S.E**, Baranyi, M, Cserepes, M, Tóvári, J. Targeting hypoxia in combination with paclitaxel to enhance therapeutic efficacy in breast and ovarian cancer. Biomed Pharmacother. 2024 Nov;180:117601. **IF: 6.9**

6. Bellini, C, Vergara, E, Bencs, F, Fodor, K, Bősze, S, Krivić, D, Bacsa, B, **Surguta, SE**, Tóvári, J, Reljic, R, Horváti, K. Design and Characterization of a Multistage Peptide-Based Vaccine Platform to Target Mycobacterium tuberculosis Infection. Bioconjug Chem. 2023 Oct 18;34(10):1738-1753. **IF: 4.0**

7. Cserepes, M, Nelhűbel, GA, Meilinger-Dobra, M, Surguta, SE, Rásó, E, Ladányi, A, Kenessey, I, Szőőr, Á, Veréb, Gy, Remenár, É, et al. Az EGFR extracelluláris módosulásainak hatása fej-nyaki daganatok cetuximabterápiájára Magyar Onkológia. 2021. 65 : 2 pp. 188-195. , 8 p.

DOI:10.14753/SE.2025.3183

10. Acknowledgements

I would like to express my sincere gratitude to my supervisor, József Tóvári, for his constant support, expert guidance, and invaluable advices throughout my PhD journey.

I would also like to express my special gratitude to Marcell Baranyi for his crucial knowledge and help in bringing this project to a success, for his useful advice in experiments, and for improving my knowledge.

I am especially grateful to all my co-authors and colleagues for their help and support, especially to Laura Svajda, Ivan Ranđelović, Mihály Cserepes, Enikő Tátrai, Kriszta Szigeti, Anita Hidvégi, Violetta Léner, Andrea Ladányi, István Kenessey and Katalin Parragné-Derecskei.

I would like to express my special thanks to Attila Kigyós, CEO of KINETO Lab, for giving me the opportunity to learn from him about industrial work and for allowing me to gain experience in this field.

Many thanks to my colleagues from the Department of Experimental Pharmacology for their invaluable support, which greatly contributed to the success of this work.

I am greatly acknowledged to Prof. Dr. Csaba Polgár and Prof. Dr.Péter Nagy, general and scientific directors of the National Institute of Oncology, for providing me the conditions to work and for allowing me to complete my PhD work at the Institute.

I would like to thank my partner Roland Parragh, for his sincere understanding and tremendous patience. I would like to thank my mother, Orsolya Surguta, for always being there to provide emotional support and encouragement; my father, András Surguta, for always helping and supporting me on my journey; my younger brother, Áron Surguta, and my older brother, Miklós Surguta, for always being there for me whenever I needed them.

DOI:10.14753/SE.2025.3183

Grant support:

This study was funded by the National Research, Development and Innovation Office (NRDIO) and Innovation Fund of the Ministry of Culture and Innovation, in the frame of the Hungarian Thematic Excellence Program (project: TKP2021-EGA-44) and the National Laboratories Program (project: National Tumor Biology Laboratory (2022-2.1.1-NL-2022-00010). Project no. 1018567 has been implemented with the support provided by the Ministry of Culture and Innovation of Hungary from the National Research, Development and Innovation Fund, financed under the KDP-2020 funding scheme. The study was supported by NRDIO's grants: NKFIH PD142272 and K-147410.